


RESEARCH

Open Access



Purine metabolism in bone marrow microenvironment inhibits hematopoietic stem cell differentiation under microgravity

Xiru Liu^{1,2,3}, Hao Zhang^{1,2,3}, Jinxiao Yan^{1,2,3}, Penghui Ye^{1,2,3}, Yanran Wang^{1,2,3}, Nu Zhang^{1,2,3}, Zhenhao Tian^{1,2,3}, Bin Liu^{4*} and Hui Yang^{1,2,3*} 

Abstract

Background Spaceflight and microgravity environments have been shown to cause significant health impairments, including bone loss, immune dysfunction, and hematopoietic disorders. Hematopoietic stem cells (HSCs), as progenitors of the hematopoietic system, are critical for the continuous renewal and regulation of immune cells. Therefore, elucidating the regulatory mechanisms governing HSC fate and differentiation in microgravity environments is of paramount importance.

Methods In this study, hindlimb unloading (HU) was employed in mice to simulate microgravity conditions. After 28 days of HU, cells were isolated for analysis. Flow cytometry and colony-forming assays were utilized to assess changes in HSC proliferation and differentiation. Additionally, transcriptomic and untargeted metabolomic sequencing were performed to elucidate alterations in the metabolic pathways of the bone marrow microenvironment and their molecular regulatory effects on HSCs fate.

Results Our findings revealed that 28 days of HU impaired hematopoietic function, leading to multi-organ damage and hematological disorders. The simulated microgravity environment significantly increased the HSCs population in the bone marrow, particularly within the long-term and short-term subtypes, while severely compromising the differentiation capacity of hematopoietic stem/progenitor cells. Transcriptomic analysis of HSCs, combined with metabolomic profiling of bone marrow supernatants, identified 1,631 differentially expressed genes and 58 metabolites with altered abundance. Gene set enrichment analysis indicated that HU suppressed key pathways, including hematopoietic cell lineage and MAPK signaling. Furthermore, integrated analyses revealed that metabolites affected by HU, particularly hypoxanthine enriched in the purine metabolism pathway, were closely associated with hematopoietic cell lineage and MAPK signaling pathways. Molecular docking simulations and in vitro experiments confirmed that hypoxanthine interacts directly with core molecules within these pathways, influencing their expression.

*Correspondence:

Bin Liu

iamicehe@163.com

Hui Yang

kittyh@nwpu.edu.cn

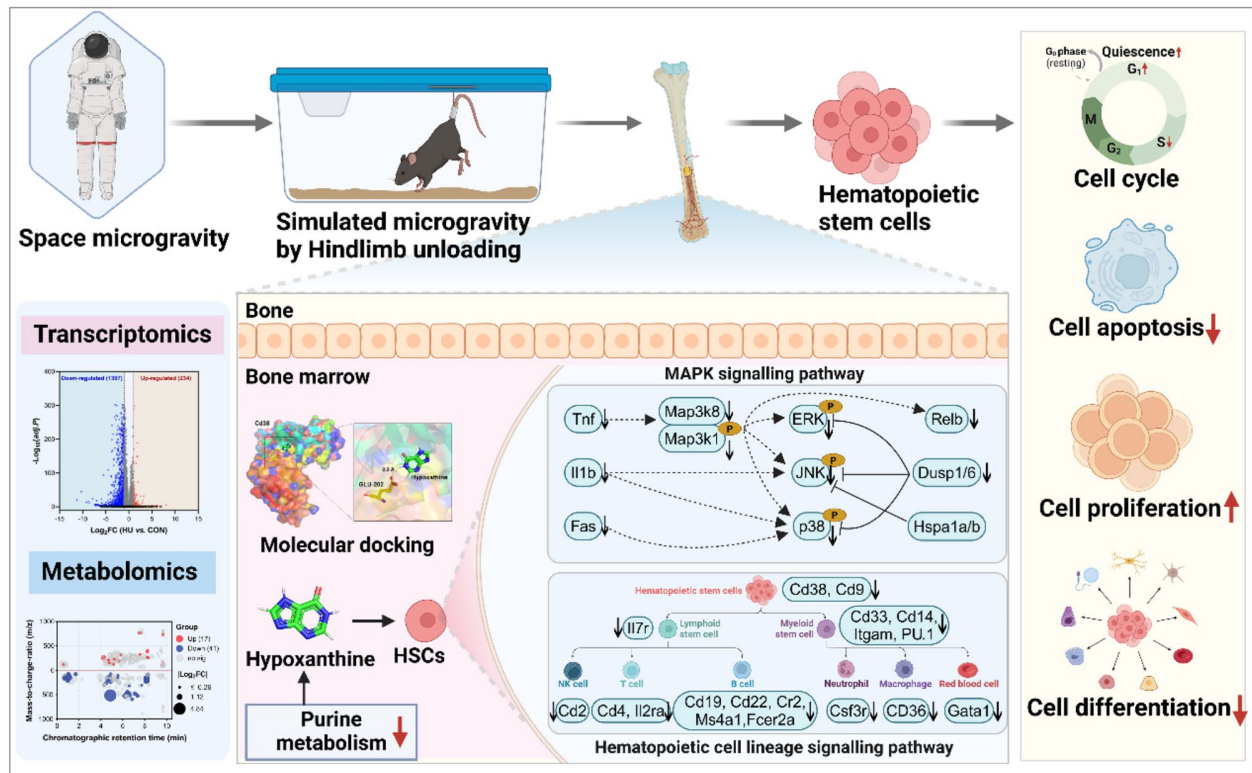
Full list of author information is available at the end of the article



© The Author(s) 2025. **Open Access** This article is licensed under a Creative Commons Attribution-NonCommercial-NoDerivatives 4.0 International License, which permits any non-commercial use, sharing, distribution and reproduction in any medium or format, as long as you give appropriate credit to the original author(s) and the source, provide a link to the Creative Commons licence, and indicate if you modified the licensed material. You do not have permission under this licence to share adapted material derived from this article or parts of it. The images or other third party material in this article are included in the article's Creative Commons licence, unless indicated otherwise in a credit line to the material. If material is not included in the article's Creative Commons licence and your intended use is not permitted by statutory regulation or exceeds the permitted use, you will need to obtain permission directly from the copyright holder. To view a copy of this licence, visit <http://creativecommons.org/licenses/by-nc-nd/4.0/>.

Conclusions These findings demonstrate that hypoxanthine in the bone marrow supernatant acts as a signaling mediator under microgravity, influencing HSCs fate by modulating hematopoietic cell lineage and MAPK signaling pathways. This study offers novel insights into the impact of microgravity on HSC fate and gene expression, underscoring the pivotal role of bone marrow microenvironmental metabolic changes in regulating key signaling pathways that determine hematopoietic destiny.

Graphical abstracts



Highlights

- Microgravity promotes the expansion of HSCs in the bone marrow by inhibiting cell cycle progression and reducing apoptosis.
- Microgravity suppresses the differentiation and function of HSPCs in the bone marrow.
- Microgravity alters purine metabolism in the bone marrow microenvironment, thereby affecting the MAPK signaling pathway and the hematopoietic cell lineage, ultimately regulating the fate of hematopoietic stem cells.

Keywords Microgravity, Hindlimb unloading, HSCs, Proliferation, Differentiation

Introduction

With the advent of long-duration space missions, the complexity of the space environment and its impact on human physiology have garnered increasing attention [1]. The space environment is characterized by extreme conditions, including high radiation, microgravity, and high vacuum [2]. Among these, microgravity exerts particularly profound effects on biological systems [3]. Research has demonstrated that microgravity can lead to immune dysfunction [4], disrupted hematopoiesis [5], and bone marrow (BM) impairment [6], thereby increasing the

risk of hematological disorders. These adverse effects are especially pronounced during extended space missions. Under microgravity, the human hematopoietic system undergoes a series of physiological changes, including impaired platelet (PLT) function, reduced lymphocyte (LYM) counts, and suppressed LYM activity. For instance, a study reported a marked decrease in the absolute number of T and B LYMs in astronauts during spaceflight [7]. However, due to limited sample sizes and significant inter-individual variability, these findings remain inconclusive.

Hematopoietic stem cells (HSCs) are critical cellular populations responsible for maintaining hematopoietic and immune homeostasis. With their high self-renewal capacity and multipotent differentiation potential, HSCs generate diverse blood cell lineages essential for normal hematopoietic function. The growth and differentiation of HSCs are primarily regulated by their BM microenvironment [8]. Previous studies have shown that microgravity significantly disrupts hematopoietic regulation, potentially altering HSC functionality by affecting cell migration, cell cycle progression, and differentiation patterns [9]. While some aspects of microgravity's impact on HSCs have been partially elucidated [10, 11], the role of BM metabolites in regulating HSC fate remains poorly understood.

Metabolites in the BM microenvironment play a critical role in precisely regulating HSC proliferation and differentiation through intricate signaling pathways. For example, fatty acids and their metabolites secreted by BM adipocytes can modulate HSC metabolic states by activating pathways such as peroxisome proliferator-activated receptor γ and sterol regulatory element-binding protein, thereby influencing HSC fate [12]. Short-chain fatty acids (e.g., butyrate and propionate) present in the BM microenvironment regulate HSC gene expression and cell cycle activity by inhibiting histone deacetylase activity and activating G protein-coupled receptors. These metabolites enhance HSC differentiation into immune cells, thereby promoting host immune homeostasis [13]. Conversely, under pathological conditions such as leukemia, certain BM metabolites (e.g., fatty acid oxidation products and squalene) promote malignant cell proliferation via the PI3K/Akt/mTOR signaling pathway while inhibiting the functionality of healthy HSCs [14]. Collectively, BM metabolites exert significant influence on HSC fate through complex metabolic and signaling networks. Investigating alterations in BM metabolites under microgravity and their interaction with HSCs is essential for elucidating HSC regulation in the spaceflight environment.

The hindlimb unloading (HU) mouse model is widely used as a ground-based analog for simulating microgravity, enabling researchers to explore physiological responses during and after spaceflight [15]. In this study, we employed the HU mouse model to investigate the effects of microgravity on HSC fate decisions. Our results revealed that microgravity induces significant alterations in the hematopoietic cell lineage, impairing HSC differentiation and regenerative capacity in HU mice. Transcriptomic and BM supernatant metabolomic analyses uncovered key molecular mechanisms by which microgravity affects HSC fate through the BM microenvironment. Notably, our findings identified purine metabolism as a critical pathway influenced by HU, which regulates

HSC differentiation via modulation of the hematopoietic and MAPK signaling pathways. These results underscore the profound impact of microgravity on HSC transcriptional regulation and the metabolic landscape of the BM. This study provides valuable insights into the mechanisms underlying hematopoietic dysfunction under spaceflight conditions and presents a novel perspective for developing intervention strategies.

The novelty of this study lies in its first systematic elucidation of the pivotal role of purine metabolism under microgravity conditions. Additionally, it proposes the hypothesis that BM metabolites regulate HSC fate through specific signaling pathways, offering fresh insights into the mechanisms underlying hematopoietic dysfunction in the spaceflight environment.

Materials and methods

Animals

The animals used in this study were 4-week-old male C57BL/6J mice (SPF grade), purchased from the Animal Experimental Center of Xi'an Jiao Tong University. The mice were housed under standard laboratory conditions with a 12-hour light/dark cycle and a controlled temperature of 23 ± 2 °C. They were provided with a standard maintenance diet (Beijing Keao Xie li Feed Co., Ltd., Beijing, China) and had unrestricted access to water. All procedures involving animals were conducted in accordance with the protocol approved by the Medical and Laboratory Animal Ethics Committee of Northwestern Polytechnical University (No. 202401196). The experimental protocols complied with ARRIVE guidelines 2.0 (Animal Research: Reporting of In Vivo Experiments).

Establishment of the HU Mouse Model

All experimental mice were acclimatized for one week before being randomly assigned to two groups. Following the protocol described by Morey-Holton et al. [16], mice in the HU group were subjected to tail suspension using a specialized apparatus to prevent hindlimb weight-bearing for 28 days. The suspension angle was maintained at 30°, allowing the mice to move freely within their cages using a pulley system. To ensure experimental consistency, the control (CON) group consisted of an equal number of mice housed individually in standard cages. Body weight was monitored weekly throughout the study. At the conclusion of the experiment, peripheral blood and BM samples were collected for analysis. Each experiment was performed in triplicate to ensure data reliability. Mice were euthanized by cervical dislocation, preceded by anesthesia induced through inhalation of an overdose of isoflurane (Ifurane, CAS: 26675-46-7). Anesthesia was only administered during the euthanasia process to minimize animal distress.

Body composition analysis

Changes in body composition were assessed using dual-energy X-ray absorptiometry scans, performed one day before euthanasia. The scans were conducted using a Lunar PIXImus II densitometer (GE Medical Systems) to measure bone mineral content (BMC) [17]. Femoral and tibial regions of the hindlimbs were analyzed specifically for BMC.

Hematoxylin and eosin (H&E) staining

Following euthanasia, select organs (heart, liver, lungs, kidneys, brain, spleen, and BM) were promptly harvested. The tissues were fixed in 4% paraformaldehyde for 48 h, embedded in paraffin, sectioned, and stained with H&E [18]. Histological images were captured using a sectioning scanner (Zhiying, Shandong, China). Spleen morphology was assessed using a scoring system based on extramedullary hematopoiesis (EMH) patterns [19]: (1) atrophy; (2) atrophic white pulp with less than 20% EMH; (3) atrophic white pulp with 20–60% EMH; (4) atrophic white pulp with 60–100% EMH; (5) early white pulp recovery with extensive EMH in red pulp; (6) well-developed white pulp with extensive EMH in red pulp; (7) normal spleen. Femur scoring system was based on the overall percentage of marrow space occupied by hematopoietic cells as compared to adipocytes and expressed as percent BM cellularity: [(marrow space occupied by hematopoietic cells/total marrow space) × 100%].

Blood counts

At the end of the 28-day experiment, whole blood samples were collected via orbital puncture. The samples were analyzed using an automated hematology analyzer (Sysmex, Shanghai, China) to measure RBC, hemoglobin (HGB), WBC, PLT, and LYM counts.

Flow cytometry analysis and cell sorting

BM cells were flushed from the femurs and tibias of mice, suspended in phosphate-buffered saline (PBS) containing 2% fetal bovine serum, and filtered to remove debris. RBCs were lysed with lysis buffer (TIANGEN, RT122-02), and BM mononuclear cells were isolated after two PBS washes [20]. HSCs were labeled with fluorophore-conjugated antibodies, including PE and FITC anti-CD3, B220, CD11b, Ter-119, and Gr-1 (eBioscience, #22-7770-72). Additional markers included PE anti-Sca-1 (clone D7, eBioscience, #12-5981-81), AF700 anti-c-kit (clone 2B8, BioLegend, #105846), APC anti-CD34 (clone MEC14.7, BioLegend, #119309), and BV421 anti-CD135 (clone A2F10, BioLegend, #135313). Cell subpopulations were identified as follows: HSCs were identified as Lin[−]Sca-1⁺c-kit⁺ (LSK), Long-term HSCs (LT-HSCs) as LSK CD34⁺CD135[−], Short-term HSCs (ST-HSCs) as (LSK CD34[−]CD135[−]), multipotent progenitors (MPPs)

as LSK CD34⁺CD135⁺, common myeloid progenitors (CMPs) as Lin[−]Sca-1[−]c-kit⁺CD34⁺CD16/32[−], granulocyte-macrophage progenitors (GMPs) as Lin[−]Sca-1[−]c-kit⁺CD34⁺CD16/32⁺, megakaryocyte-erythroid progenitors (MEPs) as Lin[−]Sca-1[−]c-kit⁺CD34[−]CD16/32[−], and common lymphoid progenitors (CLPs) as Lin[−]CD135⁺IL-7R⁺. The labeled cells were analyzed using a BD FACS Celesta flow cytometer (BD Biosciences, USA), and data were processed using FlowJo software (version 10.6.2). Gating was performed to exclude debris and mature cells, using FSC-H, FSC-A, and Lin- markers. HSCs were identified based on Sca-1⁺c-kit⁺ expression. Unstained samples, single-stained controls, and fluorescence-minus-one controls were employed to define gating boundaries.

Cell cycle analysis

The cell cycle distribution was analyzed using a Cell Cycle Analysis Kit (Beyotime Biotechnology, C1052). HSCs were washed twice with cold PBS and subsequently fixed in 70% ethanol at 4 °C overnight. The following day, cells were stained with PI at 37 °C for 30 min. Cell cycle phases (G0/G1, S, and G2/M) were assessed using flow cytometry (BD FACS Celesta, BD Biosciences, USA) and analyzed with ModFit software (version 5.0) [21].

Apoptosis analysis

Apoptosis was assessed using the Annexin V-FITC Apoptosis Detection Kit (Beyotime Biotechnology, C1062M) following the manufacturer's protocol [22]. HSCs were washed with cold PBS, then resuspended in 300 μL of binding buffer. Subsequently, 5 μL of Annexin V-FITC and 10 μL of PI were added and incubated for 1 h. After washing with PBS, the samples were analyzed by flow cytometry and FlowJo software.

Cell proliferation

Cell proliferation was evaluated using Ki67 staining [23]. Isolated HSCs were incubated with surface marker antibodies for 30 min. After washing, the cells were resuspended in fixation/permeabilization buffer (eBioscience, CA) and incubated at 4 °C in the dark for 30 min. The cells were then stained with an anti-Ki67 antibody (eBioscience, #11-5698-82) for 30 min at room temperature in the dark. Flow cytometry was used to detect Ki67-positive proliferating cells, and data were analyzed using FlowJo software.

Hematopoietic colony-formation assay

The hematopoietic colony-forming unit (CFU) assay was conducted following the manufacturer's protocol for MethoCult™ GF M3434 (STEMCELL Technologies, Canada) [24]. HSCs were suspended in MethoCult™ GF M3434 and plated in 6-well plates. The plates were

incubated at 37 °C with 5% CO₂ for 8 to12 days. After incubation, colonies were identified and counted based on the guidelines outlined in the Mouse CFU Assay Technical Manual.

RNA extraction and quantitative RT-PCR

Total RNA was extracted from sorted cells using Trizol reagent (Invitrogen, USA) and future purified with a kit

from Tiangen (China) [25]. The extracted RNA was then reverse transcribed into cDNA. Quantitative PCR was performed using the SYBR Green PCR kit (TransGen Biotech, China). Primers were synthesized by Optimus (Beijing, China), and their sequences are provided in Table 1.

[Cut]

Table 1 Primer sequence

Primer	Sequence(5' to 3')
GAPDH F	CATGGCCTTCGTTCTCCTA
GAPDH R	CCTGCTTCACCACCTTCTTGAT
Rhoa-F	CAGCAAGGACCAGTTCACAGA
Rhoa-R	AGCTGTGTCCCATAAAGCCAATC
Cdc42 F	TTCCCATCGGAATATGTACCA
Cdc42 R	CGGTCTGAGTCTGTACATAATCCTC
Yap1 F	AGCATGGTGCGCCTTGTTA
Yap1 R	CAGGCCGTGATTCAAATTTAGTG
Bmi F	ATCCCCACTTAATGTGTGCTCT
Bmi R	CTTGCTGGTCTCCAAGTAACG
TLR4 F	ATGGCATGGCTTACACCACC
TLR4 R	GAGGCCAATTTGTCTCCACA
HOXA9 F	CCCCGACTTCAGTCTTTCG
HOXA9 R	GATGCACGTAGGGGTGGTG
Tet2 F	CATTCCCACAGAGACCAGCAG
Tet2 R	GCGATGATGTACATAGGCAGCA
Gata1 F	TGGGGACCTCAGAACCCCTTG
Gata1 R	GGCTGCATTGGGGAAGTG
PU.1 F	AGGAGTCTTCTACGACCTGGA
PU.1 R	GAAGGCTTCATAGGGAGCGAT
Cd38 F	TCTCTAGGAAAGCCCAGATCG
Cd38 R	GTCCACACCAGGAGTGAGC
Cd33 F	CCGCTGTTCTTGCTGTGTG
Cd33 R	AAGTGAGCTTAATGGAGGGGTA
Il7r F	GCGGACGATCACTCTCTCTG
Il7r R	AGCCCCACATATTTGAAATCCA
Il2ra F	AACCATAGTACCCAGTTGTCCG
Il2ra R	TCCTAAGCAACGCATATAGACCA
Cd19 F	GGAGGCAATGTTGTGCTGC
Cd19 R	ACAATCACTAGCAAGATGCCC
Il1b F	GCAACTGTTCTGAACTCAACT
Il1b R	ATCTTTTGGGGTCCGTCAACT
Dusp1 F	AAGGAAAGTCCACTCTAGTCCC
Dusp1 R	GCAGGAAGTGAGATTCAAGTATG
Map3k8 F	ATGGAGTACATGACACTGGA
Map3k8 R	GGCTCTCACTTGCCATAAAGTT
Fas F	AGGTGGACTGGATACACAGAC
Fas R	TCTCCTGCCCAAACCTTTTGC
Hspa1a F	TGGTGAGTCCGACATGAAG
Hspa1a R	GCTGAGAGTCGTTGAAGTAGGC
Hspa1b F	CCGCAACAGTGTCATAGC
Hspa1b R	CCTTGAGTAATCGGAGTTGTGG
Tnf F	CTGGATGTCAATCAACAATGGGA
Tnf R	ACTAGGGTGTGAGTGTCTTCTGT

RNA-Sequencing and analysis

HSCs were sorted in triplicate from BM cells of the CON and HU groups using flow cytometry. Total RNA was extracted using RNAiso Plus (Takara, Japan) according to the manufacturer’s protocol. RNA concentration and integrity were assessed using a Qubit 2.0 fluorometer and an Agilent 2100 bioanalyzer (Novogene, China). Eukaryotic mRNA was enriched using oligo (dT)-coated magnetic beads (Novogene, China). Following cDNA synthesis and PCR amplification, the PCR products were purified using AMPure XP beads (Novogene, China) to obtain the final library. Sequencing was performed using the Illumina NovaSeq 6000 platform. Differentially expressed genes (DEGs) were identified using DESeq2 v1.6.3, with an false discovery rates (FDR) < 0.05 and $|\log_2FC| \geq 1$. Gene Ontology (GO) and Kyoto Encyclopedia of Genes and Genomes (KEGG) pathway enrichment analyses of DEGs were conducted using the DAVID database, and Gene Set Enrichment Analysis (GSEA) was applied for functional gene set enrichment.

Untargeted metabolomics

BM supernatant samples of mouse were collected, and metabolites were extracted from samples using a pre-cooled 50% methanol buffer, then stored at – 80 °C prior to liquid chromatograph mass spectrometer (LC-MS) analysis. Chromatographic separation was performed on an ultra-performance liquid chromatography (UPLC) system (SCIEX, UK) using a reversed-phase ACQUITY UPLC T3 column (100 mm × 2.1 mm, 1.8 μm, Waters, UK). The column oven was maintained at 35 °C, with a flow rate of 0.4 mL/min. Both positive (ionspray voltage at 5000 V) and negative ion modes (– 4500 V) were analyzed using a TripleTOF 5600 Plus high-resolution tandem mass spectrometer (SCIEX, UK). Mass spectrometry data were acquired in Interactive D Time-of-Flight Assembler Professional mode, with a time-of-flight mass range of 60 to 1200 Da. Survey scans were collected in 150 milliseconds, and product ion scans were collected for up to 12 cycles with a total cycle time of 0.56 s. Rigorous quality assurance procedures included mass accuracy calibration every 20 samples and a quality control sample every 10 samples. LC-MS raw data were processed using XCMS (Scripps, La Jolla, CA) for peak picking, alignment, gap filling, and normalization. Metabolite annotation was performed using the KEGG database by

matching the precise molecular mass data (m/z) to the database entries.

Enzyme linked immunosorbent assay (ELISA)

BM supernatant samples from each group were collected following centrifugation, and hypoxanthine levels were measured using an ELISA kit (LANSO, China) strictly following the manufacturer's protocol.

Statistical analysis

Statistical analysis was performed using GraphPad Prism 9.0.2 software. All data were expressed as the mean \pm standard error of the mean (SEM). Comparisons among multiple groups were conducted with one-way analysis of variance (ANOVA) or two-way ANOVA (Tukey's multiple comparisons test). Two-tailed *Student's* *t*-test was used to compare the data between the two groups. Comparisons were considered significant when $P < 0.05$.

Results

Simulated microgravity induces multiple organ injury and peripheral blood abnormalities in mice

The effects of microgravity on hematopoiesis represent a critical area of ongoing research. However, progress has been hindered by limitations in research samples. The HU model is a classical method for simulating microgravity on Earth. This model effectively replicates the physiological conditions of humans in a microgravity environment in model organisms while allowing for prolonged monitoring. In this study, we treated mice for 28 days using this method. Our results demonstrated a substantial decrease in body weight during the first week of treatment in the HU group (Fig. 1A). Although their body weight remained markedly lower than that of the control (CON) group throughout the subsequent three weeks, the rate of weight gain was comparable between the two groups (Fig. 1A, B). Previous studies have shown that weightlessness leads to bone loss. Consistent with these findings, bone mineral density scans revealed a significant reduction in BMC in the hind limbs of the HU group (Fig. 1C).

Furthermore, histological evaluations were conducted on significant organs of the mice using H&E staining. The findings demonstrated that, compared to the CON group, the HU group exhibited myocardial fiber rupture and disorganized cellular architecture, marked vacuolization in the liver, widened interstitial spaces in lung tissue, disorganized fibrous structures in the kidneys, and inflammatory cell infiltration in the brain tissue (Fig. 1D). Additionally, peripheral blood analysis revealed significant reductions in WBC and LYM in the HU group. In contrast, RBC and HGB levels were significantly elevated, with no notable changes in PLT counts (Fig. 1E). These

observations are consistent with changes observed in astronaut post-spaceflight, confirming that a microgravity environment can induce peripheral blood abnormalities [26]. Our findings indicate that microgravity exerts a significant adverse impact on overall health.

Simulated microgravity alters the structure of the BM cavity and the proportional distribution of HSCs subpopulations

Based on the observed abnormalities in peripheral blood induced by simulated microgravity, we further evaluated its effects on HSCs. Histological analysis via H&E staining revealed a significant reduction in the spatial occupancy of BM, the primary niche for HSCs, following HU treatment (Fig. 2A). In addition, HU treatment led to a marked expansion of the splenic red pulp and a significant reduction in extramedullary hematopoiesis scores (Fig. 2B). Flow cytometry analysis of LSK cell populations showed that HU treatment significantly increased the proportion of LSK cells. Within this population, the ratios of LT-HSCs and ST-HSCs markedly elevated, while the proportion of MPPs significantly reduced (Fig. 2C). Moreover, compared to the CON group, HSCs in the HU group exhibited a decreased apoptosis rate (Fig. 2D), cell cycle arrest (evidenced by an increase in G0/G1 phase cells and a decrease in S phase cells) (Fig. 2E), and enhanced proliferative activity (indicated by a higher ratio of Ki67-positive cells) (Fig. 2F). Previous studies have suggested that Rhoa and Cdc42 regulate cell proliferation through cyclin modulation, while the activation of Yap1, Bmi, TLR4, HOXA9, and Tet2 promotes HSCs proliferation and differentiation. RT-PCR analysis in this study demonstrated significant upregulation of Cdc42, Yap1, Bmi, TLR4, HOXA9, and Tet2 expression in HSCs from the HU group compared to the CON group (Fig. 2G). These results indicate that simulated microgravity enhances the survival and proliferation of HSCs, thereby sustaining their hematopoietic potential.

Simulated microgravity inhibits the differentiation of HSCs into downstream cell lineages

To further investigate the effects of microgravity on HSCs differentiation, we employed flow cytometry to analyze various downstream cell lineages of MPPs. The results demonstrated a significant reduction in the proportion of CMP, CLP, and MEP in HU group, while no significant change was observed in GMP compared to the CON group (Fig. 3A-B). Next, we assessed the impact of HU on HSCs differentiation potential through colony-forming assays. The data revealed that HU treatment markedly suppressed the total number of hematopoietic colonies, including a significant reduction in CFU granulocyte-erythrocyte-macrophage-megakaryocyte (CFU-GEMM), CFU granulocyte-macrophage (CFU-GM),

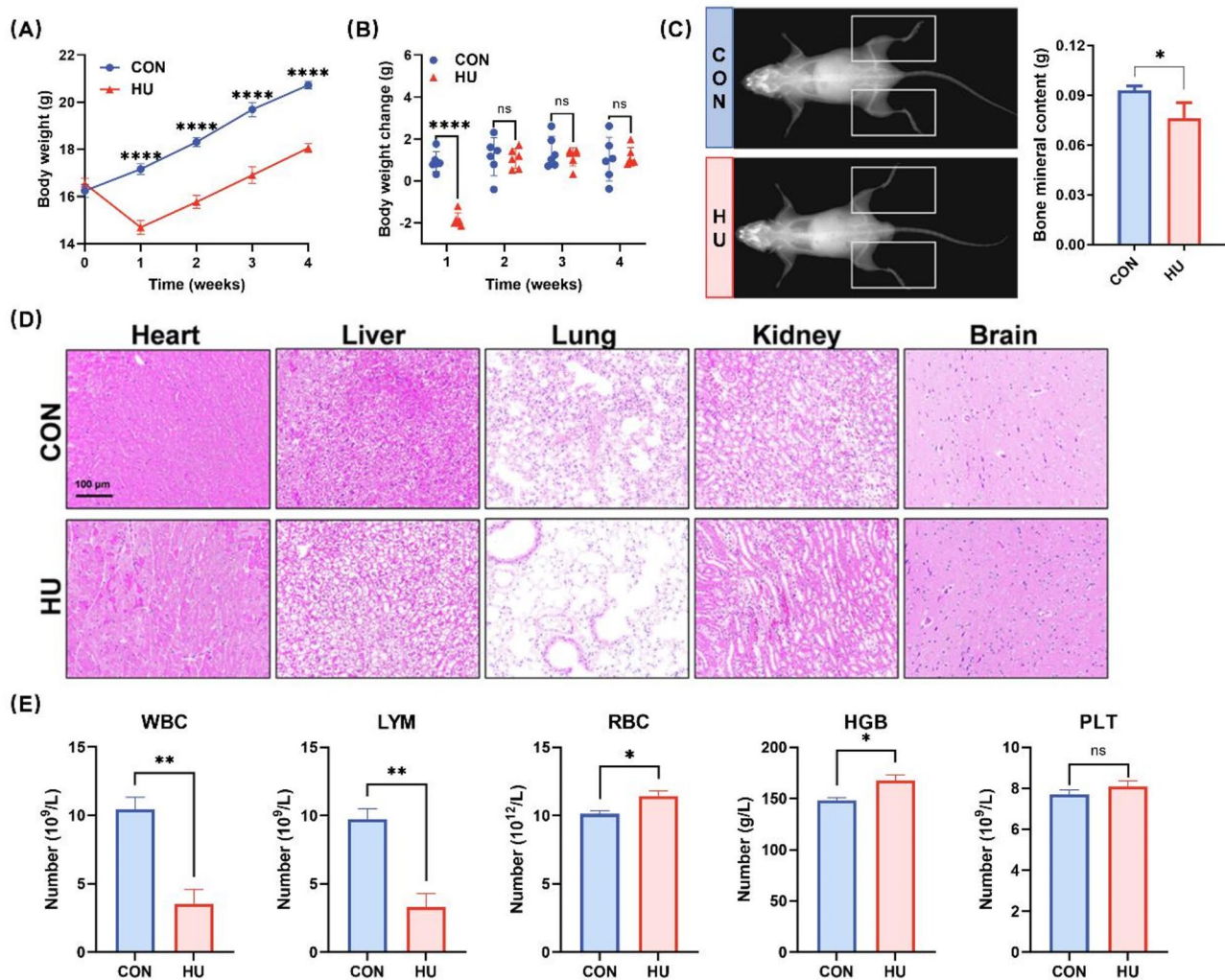


Fig. 1 Effects of simulated microgravity on organ systems and hematological profile in mice. **(A-B)** Growth curves of body weight during the experimental period for the control (CON) and hindlimb unloading (HU) groups **(A)**, and weekly changes in body weight **(B)**. **(C)** Representative images and statistical analysis of hind limb bone mineral density scans following hindlimb unloading in mice. **(D)** Representative H&E staining images of heart, liver, lung, kidney, and brain tissues from the two groups, with a scale bar of 100 μ m. **(E)** Peripheral blood analysis results, including white blood cell (WBC), lymphocyte (LYM), red blood cell (RBC), hemoglobin (HGB), and platelet (PLT) counts. Statistical analysis evaluates hematological differences between the CON and HU groups. Data are presented as mean \pm SEM ($n=6$). Statistical significance was determined using two-way ANOVA (Tukey's multiple comparisons test) for **(A)**, and two-tailed Student's *t*-tests for **(B-E)**. * $P < 0.05$, ** $P < 0.01$, **** $P < 0.0001$, and ns (not significant) $P \geq 0.05$

and Burst-forming unit-erythroid (BFU-E) colony formation (Fig. 3C-D). Furthermore, during HSCs differentiation, Gata1 is closely associated with erythroid and megakaryocytic lineage commitment, while PU.1 is a pivotal transcription factor regulating myeloid and lymphoid differentiation. Our RT-PCR analysis showed that the expression levels of Gata1 and PU.1 in HSCs from the HU group were significantly lower than those in the CON group (Fig. 3E). These findings indicate that simulated microgravity inhibits the differentiation of HSCs into downstream HSPC lineages, potentially enabling HSCs to retain their stemness, as illustrated in Fig. 3F.

Simulated microgravity altered the transcriptional profile of HSCs

To evaluate the impact of microgravity on gene expression patterns associated with HSCs differentiation, we collected BM-derived HSC samples from the CON and HU groups for RNA sequencing on day 28. Principal component analysis (PCA) and sample similarity analysis revealed that the distances between samples within the CON and HU groups were comparable, while significant differences existed between the groups, indicating that HU treatment altered the transcriptome of HSCs (Fig. 4A-B). A total of 1631 DEGs were identified, with 234 significantly upregulated and 1397 significantly downregulated ($|\log_2FC| > 1$, *adjust.P* < 0.05 ; Fig. 4C and

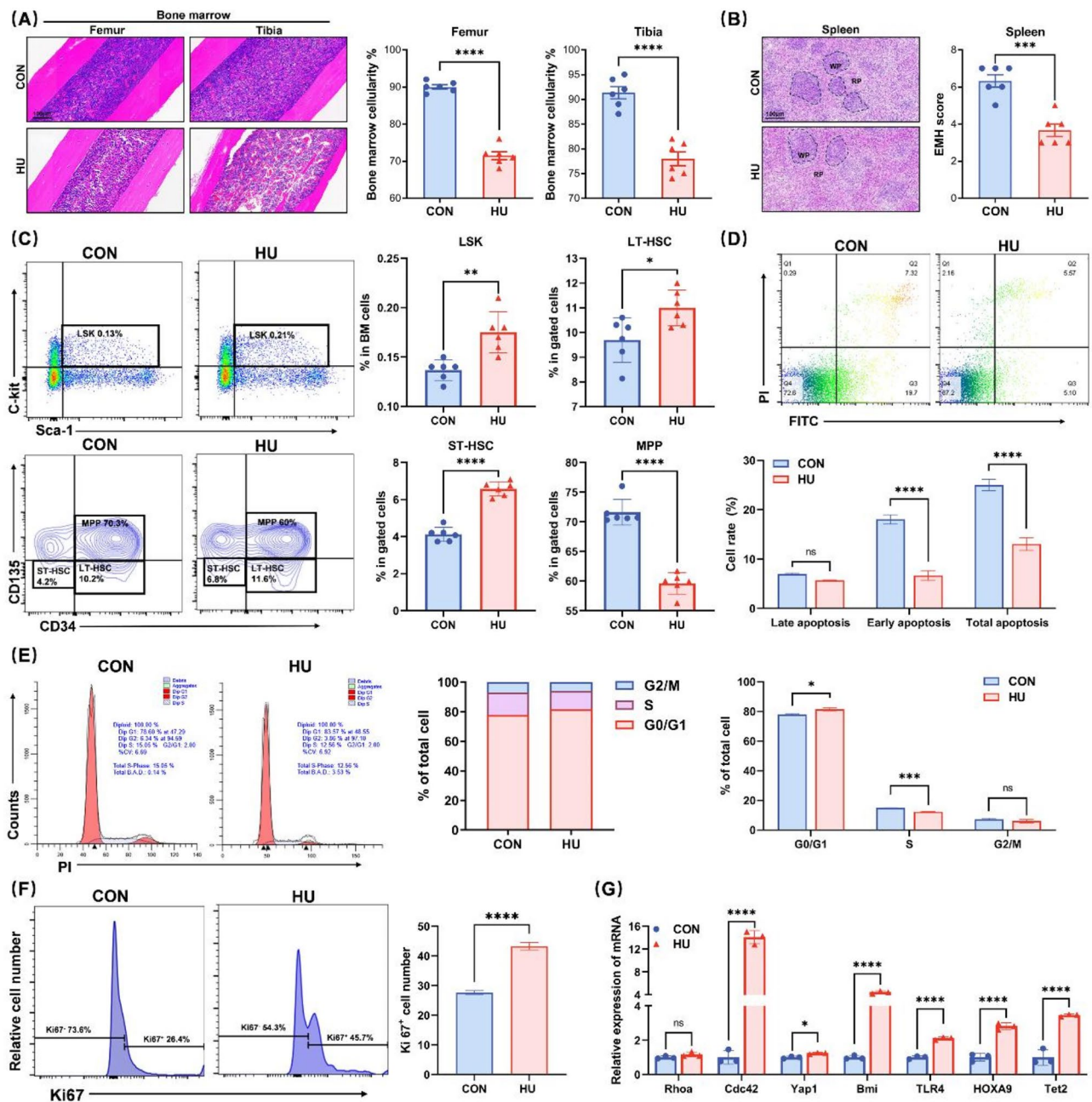


Fig. 2 Enhanced proliferation of HSCs under simulated microgravity conditions. **(A)** Representative H&E staining images of femurs and tibias from control (CON) and hindlimb unloading (HU) mice are shown, along with quantification scores of bone marrow cellularity. **(B)** Representative H&E staining images of spleen tissue. Scoring for hematopoiesis was conducted based on the distribution and density of hematopoietic cells. The white pulp (WP) is delineated by black dashed circles, while red pulp (RP) corresponds to the areas outside the WP. **(C)** Flow cytometric analysis of HSC populations in BM. Upper panel: Representative images and frequency statistics of LSK (Lineage[−]Sca-1⁺c-Kit⁺) cells in BM. Lower panel: Representative images and proportion statistics for LT-HSCs (long-term HSCs), ST-HSCs (short-term HSCs), and MPP (multipotent progenitors) within the LSK population. **(D)** Representative images and quantification of apoptotic HSCs from flow cytometric analysis. **(E)** cell cycle distribution and statistical analysis of HSCs between CON and HU groups. **(F)** Proliferative activity of HSCs: Ki67⁺ cells and statistical comparison between CON and HU groups. **(G)** RT-PCR was performed to assess the expression of key proliferation-related genes in LSK cells isolated from BM. Expression levels of target genes were normalized and compared between CON and HU groups. Data are presented as mean ± SEM (**A–F**: $n = 6$; **G**: $n = 3$). Statistical significance was assessed using two-tailed Student's *t*-tests. * $P < 0.05$, ** $P < 0.01$, *** $P < 0.001$, **** $P < 0.0001$, and ns (not significant) $P \geq 0.05$

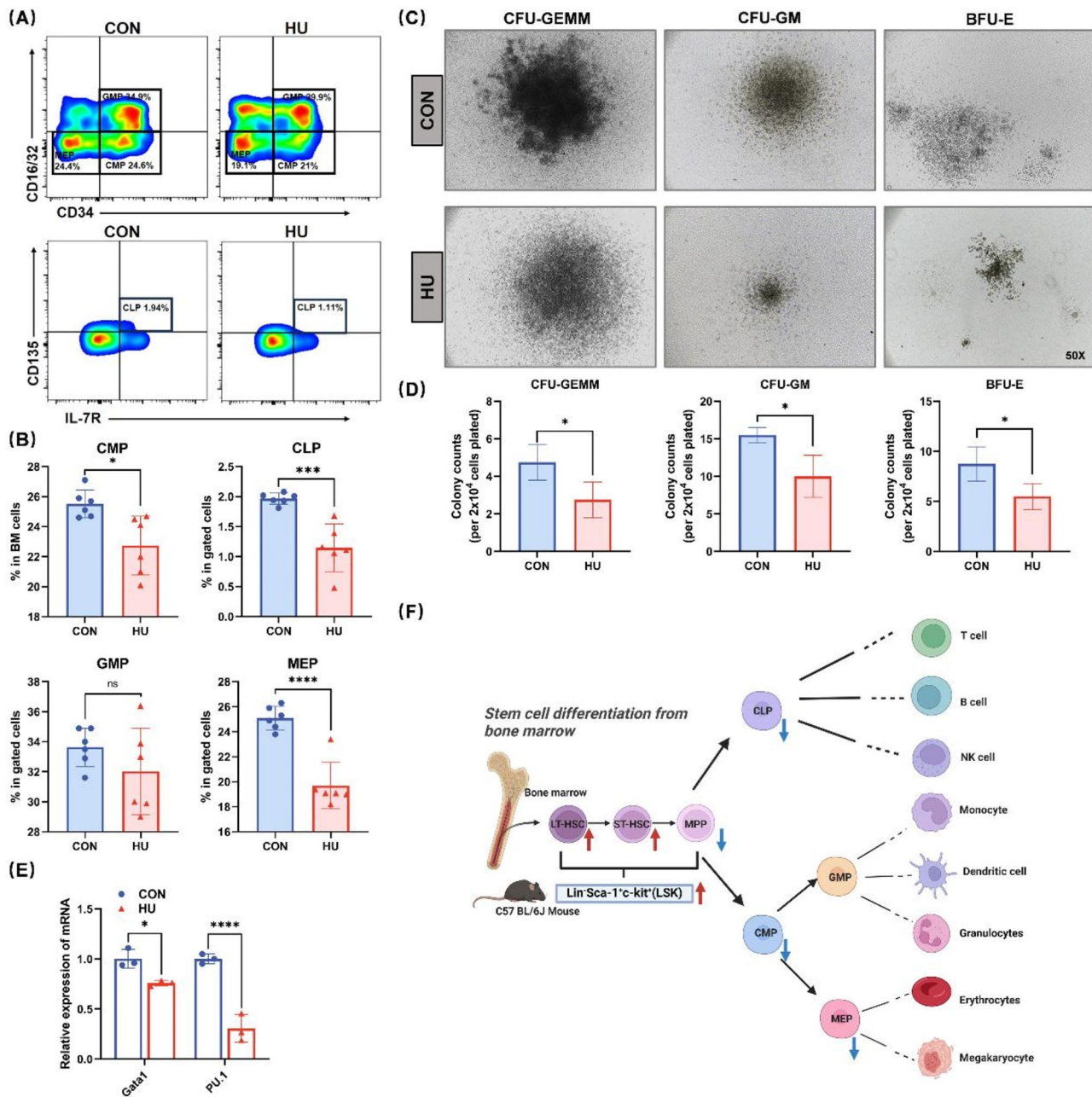


Fig. 3 Inhibitory effects of simulated microgravity on hematopoietic stem and progenitor cell (HSPC) differentiation. **(A–B)** Flow cytometric analysis of myeloid progenitor cell populations in LK cells (Lineage⁻c-Kit⁺): Representative flow cytometry plots **(A)** and statistical data **(B)** illustrate the proportion of granulocyte-monocyte progenitors (GMP), megakaryocyte-erythroid progenitors (MEP), and common myeloid progenitors (CMP) in BM cells from control (CON) and hindlimb unloading (HU) mice. **(C)** Representative images (50x objective magnification) of CFUs cultured for 8 days from HSCs isolated from CON and HU mice. Images demonstrate distinct morphological characteristics and colony densities under the two conditions. **(D)** Quantitative analysis on the proportion of CFU-GEMM (granulocyte-erythrocyte-monocyte-megakaryocyte), CFU-GM (granulocyte-monocyte), and BFU-E (burst-forming unit-erythroid) colonies. **(E)** RT-PCR analysis of key gene expression levels related to HSPC differentiation. **(F)** HSC differentiation hierarchy and lineage changes under simulated microgravity exposure. Red upward arrows indicate an increase, while blue downward arrows indicate a decrease in the HU group compared to the CON group. Data are presented as mean ± SEM (**A–D**: $n = 6$; **E**: $n = 3$). Statistical significance was assessed using two-tailed Student's *t*-tests. * $P < 0.05$, ** $P < 0.01$, *** $P < 0.001$, **** $P < 0.0001$, and ns (not significant) $P \geq 0.05$

Supplementary Table S1). The expression patterns of the top 10 upregulated and downregulated genes are shown in Fig. 4D. Subsequently, we conducted GO enrichment analysis on the DEGs. In the biological process (BP)

category, a total of 121 terms were enriched, with the top five being immune system process, immune response, inflammatory response, innate immune response, and response to lipopolysaccharide. Cell component (CC)

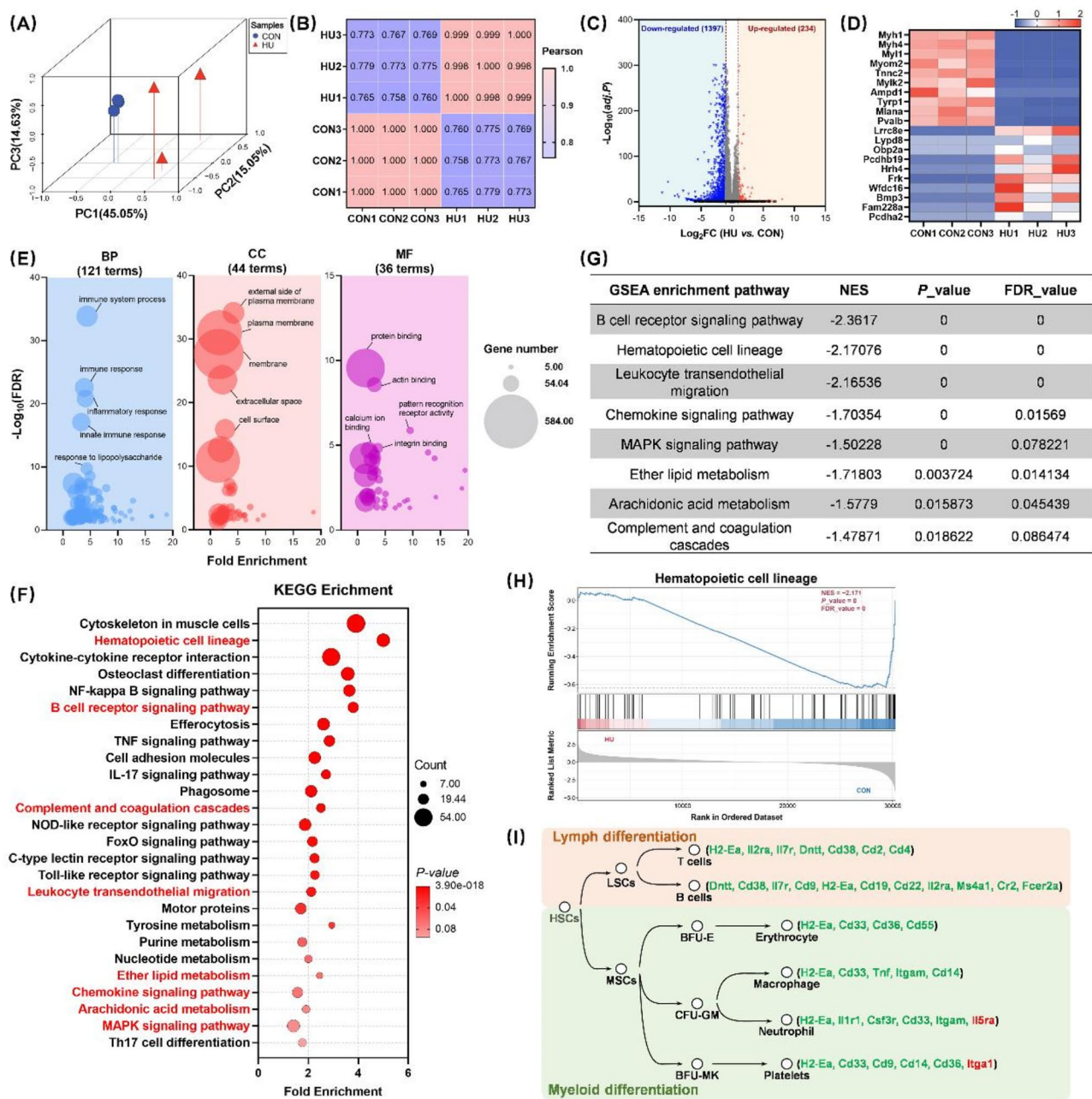


Fig. 4 RNA-seq analysis of HSCs from the HU and CON groups. **(A–B)** Principal component analysis (PCA) of the transcriptional profiles **(A)** and Pearson's correlation-based analysis **(B)** of each sample in the control (CON) and hindlimb unloading (HU) groups. PCA demonstrates the positioning of samples in a three-dimensional coordinate system. **(C)** Visualization of differentially expressed genes (DEGs) in the HU group compared to the CON group. Red indicates upregulated genes, and blue indicates downregulated genes. **(D)** Heatmap of the top 10 upregulated and downregulated DEGs. **(E)** GO enrichment analysis of DEGs, displaying the enriched pathways under three categories: Biological Process (BP), Cellular Component (CC), and Molecular Function (MF). The size of the points represents the number of genes enriched in each pathway, with labels indicating the top five pathways in each category. **(F)** KEGG enrichment analysis of DEGs. Pathways shared with the GSEA analysis of DEGs are highlighted in red. **(G)** GSEA enrichment data for the shared KEGG and GSEA pathways. **(H–I)** GSEA enrichment results visualization for Hematopoietic cell lineage **(H)** and a manually drawn pathway diagram from KEGG **(I)**. The molecular markers of each cell type are annotated, with color-coded changes in expression between the HU and CON groups: green indicates downregulation, and red indicates upregulation

analysis revealed 44 enriched terms, with the top five being external side of plasma membrane, plasma membrane, membrane, extracellular space, and cell surface. Molecular function (MF) analysis identified 36 enriched terms, with the top five being protein binding, actin binding, pattern recognition receptor activity, integrin binding, and calcium ion binding (Fig. 4E and Supplementary Table S2). Furthermore, we performed KEGG pathway enrichment and GSEA on the DEGs to investigate the signaling pathways through which HU regulates HSCs differentiation. The KEGG bubble chart highlighted eight enriched pathways common to both analyses, including hematopoietic cell lineage, B cell receptor signaling pathway, complement and coagulation cascades, leukocyte transendothelial migration, ether lipid metabolism, chemokine signaling pathway, arachidonic acid metabolism, and MAPK signaling pathway (Fig. 4F and Supplementary Table S3). GSEA results indicated that the normalized enrichment scores (NES) for these eight pathways were all negative, suggesting that HU treatment suppressed the activity of these pathways (Fig. 4G and Supplementary Table S4). Notably, the hematopoietic cell lineage exhibited a higher level of enrichment among these pathways (KEGG: $P < 0.0001$, Fold Enrichment = 5.0; GSEA: FDR = 0, NES = -2.171). The GSEA results, along with pathway visualization, further indicated that HU treatment inhibited the pathway activity during the differentiation process of HSCs and reduced the expression of downstream cell surface markers (Fig. 4H-I). These transcriptomic characteristics suggest that the differentiation capacity of HSCs in HU mice is significantly impaired.

Simulated microgravity disrupts the metabolic balance of the BM supernatant

HSCs are predominantly located within the BM, where metabolites in the BM supernatant serve as essential regulatory components of the microenvironment that supports HSCs survival. Studies have shown that these proximal molecular signals not only influence HSCs proliferation and differentiation but also play a pivotal role in determining cell fate. To investigate whether microgravity alters the metabolism of the BM microenvironment, we conducted untargeted metabolomics sequencing to identify metabolites in the BM supernatant of mice. A total of 21,262 feature peaks were detected in both negative and positive ion modes. After merging and MS2 matching, 303 metabolites were identified. Orthogonal partial least squares discriminant analysis (OPLS-DA) revealed a clear separation between the CON and HU groups (Fig. 5A). A 100-permutation test on the OPLS-DA model confirmed its strong classification performance without overfitting ($R^2Y = 0.997$, $Q^2Y = 0.685$). We identified 58 differentially accumulated metabolites

(DAMs), of which 41 were significantly downregulated, and 17 were significantly enriched in the HU group (Fig. 5B and Supplementary Table S5). Functional classification based on the HMDB database indicated that the metabolites most significantly affected by simulated microgravity included phospholipids (12), acyl groups (9), benzene derivatives (6), pyridines and derivatives (3), organonitrogen compounds (3), carboxylic acids and derivatives (3), and imidazopyrimidines (3), as shown in Fig. 5C. Further pathway topology analysis revealed that the DAMs significantly affected by microgravity were primarily involved in purine metabolism, primary bile acid biosynthesis, and taurine and hypotaurine metabolism (Fig. 5D and Supplementary Table S6). Moreover, KEGG enrichment analysis underscored the pivotal role of purine metabolism in the metabolic alterations observed in the BM microenvironment under simulated microgravity (Fig. 5E).

Integrated omics analysis reveals a close association between HU-induced disruptions in BM supernatant metabolism and transcriptomic alterations in HSCs

To investigate whether the impact of HU treatment on HSCs fate is related to metabolic alterations in the BM microenvironment, we conducted a correlation analysis on 58 DAMs and 778 DEGs identified post-HU treatment (including only KEGG-annotated genes). Pearson correlation analysis revealed a significant association between the transcriptomic profile of HSCs and the metabolic profile of BM supernatant (Fig. 6A; $|\text{Rho}| \geq 0.85$, $P < 0.05$). Further pathway enrichment analysis based on the KEGG database identified eight commonly enriched metabolic pathways, including purine metabolism, glutamate metabolism, folate metabolism, and phospholipid metabolism, with purine metabolism showing the highest degree of enrichment (Fig. 6B). Figure 6C illustrates the co-enriched DEGs and DAMs involved in purine metabolism, where key enzymes *Entpd1*, *Entpd3*, and *Nt5e*, involved in adenine and guanine metabolism, were downregulated following HU treatment. Additionally, the key enzyme *Xdh*, involved in hypoxanthine and xanthine metabolism, was suppressed by HU, with its expression significantly positively correlated with the abundance of its respective substrates (Fig. 6C).

Given the complexity of the relationship between metabolites and gene expression, we further analyzed the correlations between key metabolites (enriched in the metabolic pathways identified) and key genes (enriched in the eight signaling pathways from the transcriptomic analysis). Results indicated that most DAMs were significantly correlated with DEGs involved in the eight core signaling pathways, particularly hypoxanthine and xanthine within purine metabolism, which showed a positive correlation with downregulated DEGs and a negative

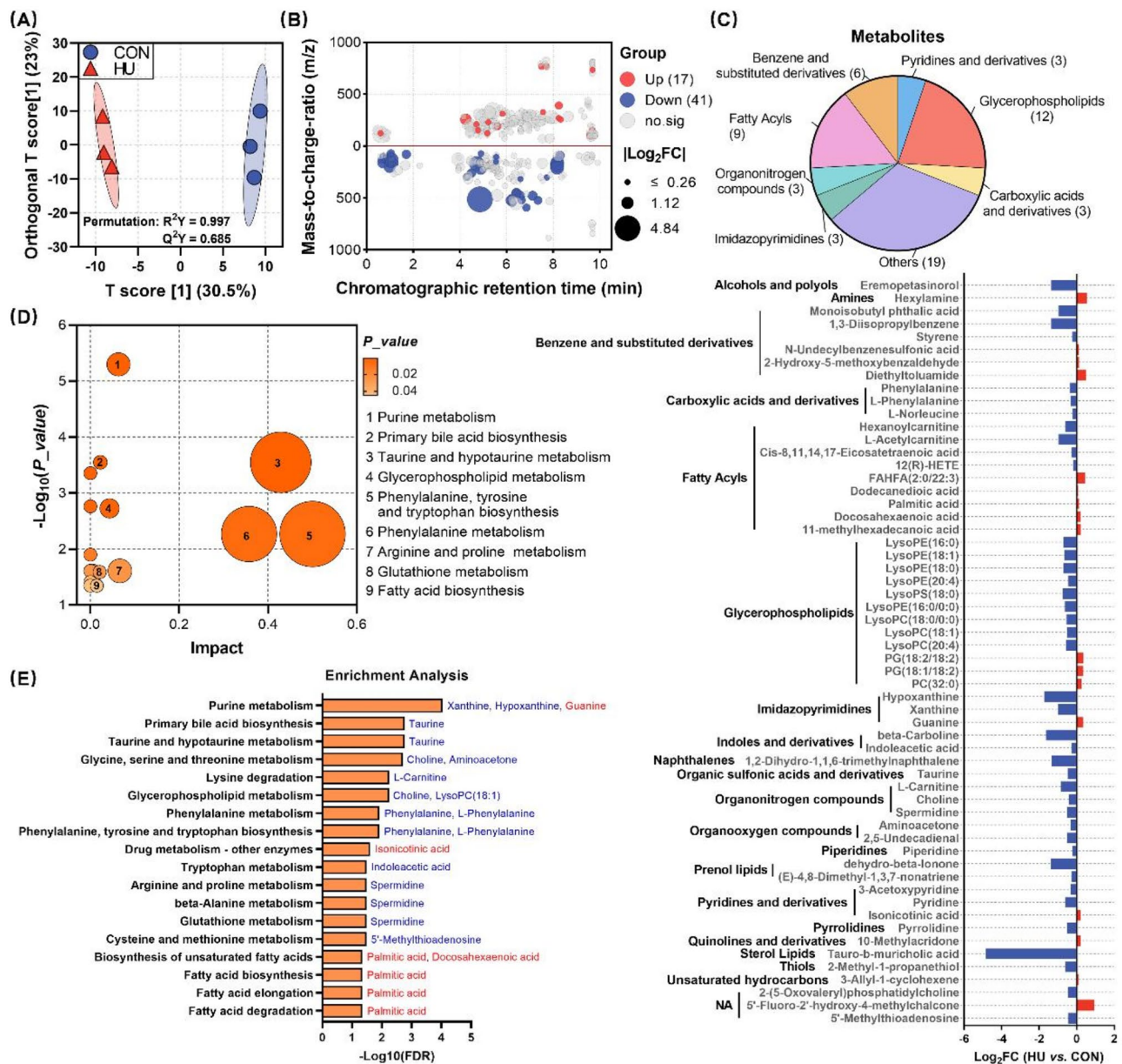


Fig. 5 Untargeted metabolomics analysis of BM supernatant samples from the CON and HU groups. **(A)** Orthogonal partial least squares-discriminant analysis (OPLS-DA) score plot of BM supernatant metabolic profiles from the control (CON) and hindlimb unloading (HU) groups. Differences in metabolic patterns between groups were statistically validated using permutation tests. **(B)** Total ion chromatograms of annotated metabolites detected via MS2. Differentially abundant metabolites (DAMs) in the HU group compared to the CON group are color-coded: red (upregulated), blue (downregulated), and gray (no significant difference). **(C)** Classification and distribution of DAMs. Pie chart showing DAM classification. A bar chart visualizes their fold changes and their distribution in the HU group. **(D)** Pathway topology analysis of DAMs. Dot size and color intensity represent pathway importance, with larger and darker dots indicating greater significance. **(E)** Pathway enrichment analysis of DAMs. Metabolites enriched in each pathway are listed. Font color indicates the direction of change under simulated microgravity: red (increased), blue (decreased)

correlation with upregulated DEGs under HU treatment (Fig. 6D). Overall, these findings suggest that microgravity may alter the transcriptomic profile of HSCs by modulating metabolites within the BM microenvironment, thus influencing their proliferation and differentiation.

Hypoxanthine restores HU-Induced downregulation of hematopoietic and MAPK pathway genes in BM

Hypoxanthine emerged as the most significantly affected metabolite in purine metabolism under HU treatment, with strong associations to the eight altered signaling pathways ($\log_2FC = -1.738$; Fig. 5C). Among these pathways, the hematopoietic cell lineage and MAPK signaling

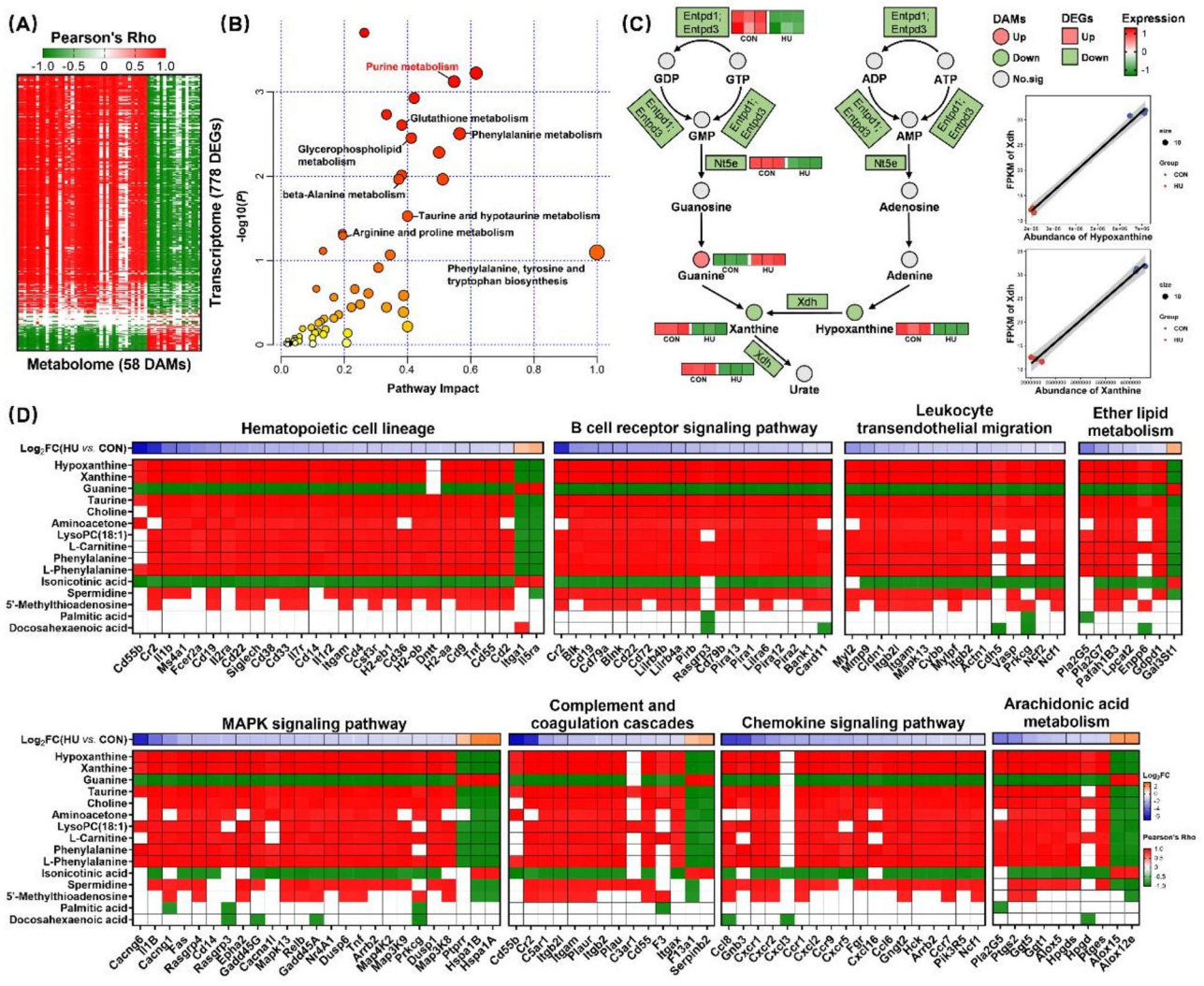


Fig. 6 Integrated correlation analysis of the transcriptome and metabolome. **(A)** Pearson correlation analysis identifies significant associations between 58 differentially abundant metabolites (DAMs) and 778 differentially expressed genes (DEGs). The correlation matrix highlights positive and negative correlations, with the strength of associations represented by color gradients. **(B)** Bubble plot displays the results of integrated pathway enrichment analysis combining transcriptomic and metabolomic data. Pathways with significant enrichment are shown, with bubble size representing the impact value and color intensity reflecting statistical significance (P -value). **(C)** Adenine metabolism pathway expression profiles. The expression levels of key metabolites and genes involved in the adenine metabolism pathway are shown for the CON and HU groups. Expression patterns highlight changes induced by microgravity. Xdh (xanthine dehydrogenase) expression is positively correlated with hypoxanthine levels ($R=0.9972$, $P<0.0001$) and xanthine levels ($R=0.9957$, $P<0.0001$). **(D)** Pathway-specific correlation analysis. Correlation analysis across eight signaling pathways identifies associations between differential genes and metabolites. Results are visualized through heatmaps, with key pathways such as purine metabolism and MAPK signaling prominently displayed. Strong correlations ($P<0.05$ and $|\text{Rho}|>0.85$) are highlighted with colors: red indicates positive correlations, and green indicates negative correlations

pathways contained the highest number of DEGs, with substantial evidence from the literature supporting the roles of these pathways in regulating HSCs proliferation and differentiation. Therefore, we further employed molecular docking to determine the interactions between hypoxanthine and key genes within the hematopoietic cell lineage and MAPK signaling pathways. Hypoxanthine could form hydrogen bonds with essential molecules in the hematopoietic cell lineage, including Cd38, Cd33, Il7r, Il2ra, and Cd19, as well as with DEGs in the

MAPK signaling pathway, such as Il1b, Dusp1, Map3k8, Fas, Hspa1a, Hspa1b, and Tnf. The binding free energies were all below 5 kcal/mol, indicating a high affinity for these interactions (Fig. 7 and Table 2). These findings suggest that HU-affected hypoxanthine may influence HSCs proliferation and differentiation by modulating signal transduction through molecular interactions with core molecules within these critical pathways.

[Cut]

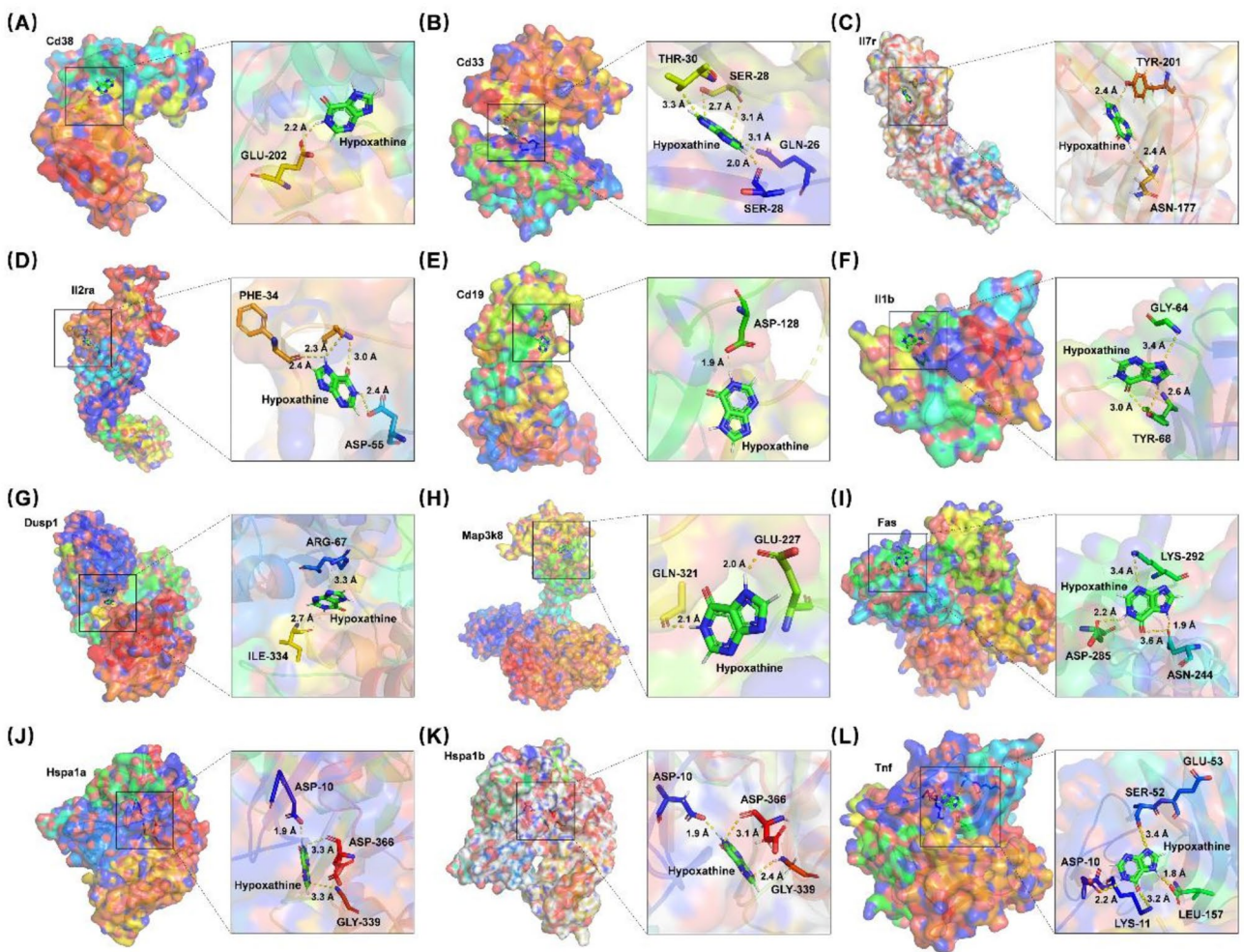


Fig. 7 The molecular docking results between hypoxanthine and key molecules in the hematopoietic cell lineage and MAPK signaling pathways. **(A–E)** The molecular docking results of hypoxanthine with critical molecules in the hematopoietic cell lineage pathway, including Cd38, Cd33, Il7r, Il2ra, and Cd19. **(F–L)** The docking results between hypoxanthine and key molecules in the MAPK signaling pathway, such as Il1b, Dusp1, Map3k8, Fas, Hspa1a, Hspa1b, and Tnf. For each docking diagram, the left panel displays the relative positioning of hypoxanthine and the protein within the binding pocket, while the right panel provides a detailed depiction of the binding pocket. The protein is shown with its surface structure, and hypoxanthine along with the amino acid residues involved in the binding are represented as stick models. The hydrogen bonds between the two are shown as yellow dashed lines, with the bond length labeled for each interaction

Table 2 The score of molecular docking		
Legend	Target (Gene name-Entry ID)	Estimated ΔG (kcal/mol)
Hypoxanthine	CD38-2eg9	-6.292646
	IL7R-4nn5	-5.9945645
	IL1B-8i1b	-6.1699977
	FAS-3oq9	-6.6770782
	TNF-7kpb	-6.5223403
	CD19-6al5	-6.3063345
	DUSP1-6d66	-6.346237
	IL2RA-3iu3	-6.6211867
	HSPA1B-7f4x	-6.5046544
	HSPA1A-5bn8	-6.611462
	MAP3K8-4y85	-6.7112846
	CD33-6d4a	-6.1019273

To further confirm the accuracy of these findings, ELISA experiments revealed a decrease in hypoxanthine concentration in BM following HU treatment (Fig. 8A). Subsequently, we treated mouse BM cells with 100 pg/mL hypoxanthine for three days and measured the expression of genes related to the hematopoietic cell lineage and MAPK signaling pathways using quantitative RT-PCR. The results indicated that HU treatment significantly downregulated the expression of Cd38, Cd33, Il7r, Il2ra, and Cd19 in the hematopoietic cell lineage signaling pathway, as well as Il1b, Dusp1, Map3k8, Fas, Hspa1a, Hspa1b, and Tnf in the MAPK signaling pathway (Fig. 8B–M). After adding hypoxanthine, the expression of these genes at the mRNA level was significantly restored and enhanced. These findings suggest that HU modulates key genes involved in hematopoietic differentiation and

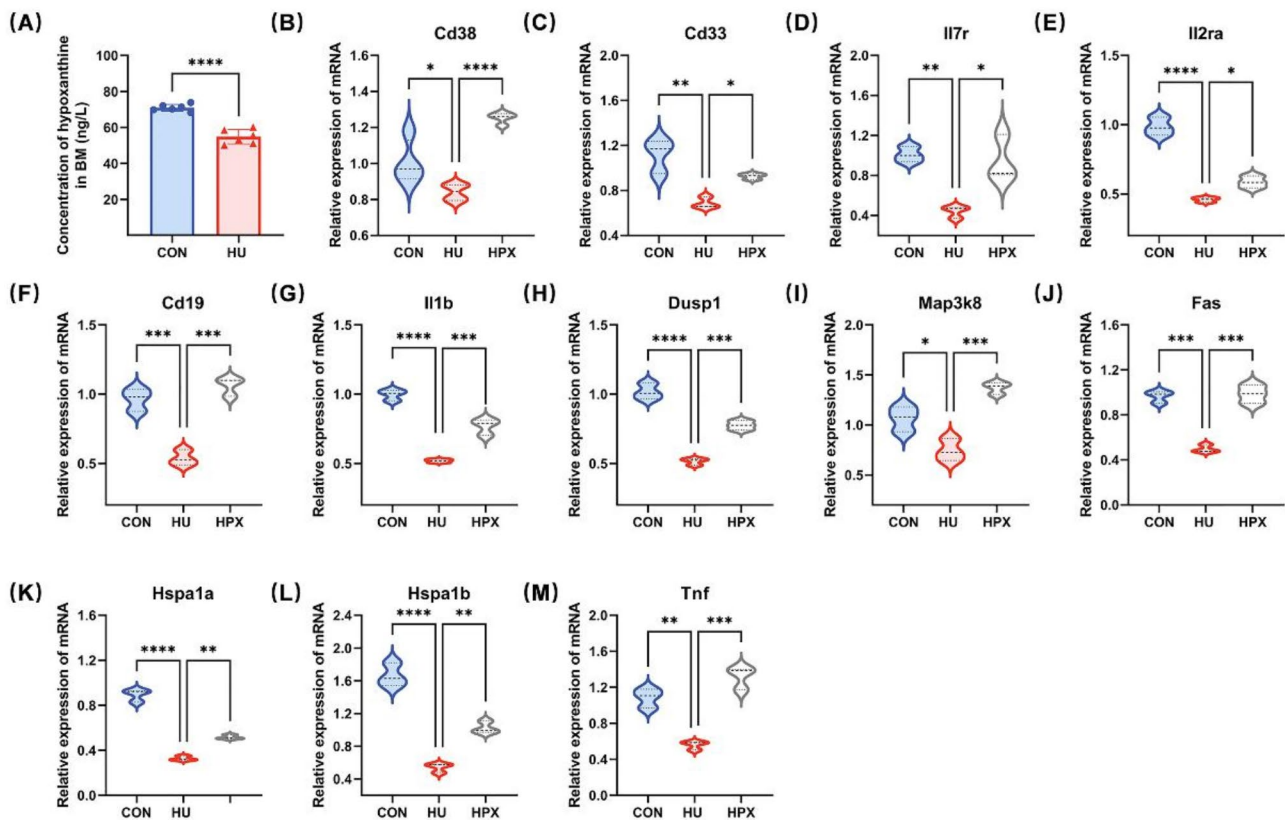


Fig. 8 The effects of hypoxanthine on the hematopoietic cell lineage and MAPK signaling pathways. **(A)** ELISA assay results showing the concentration of hypoxanthine in the bone marrow (BM). **(B-F)** Relative mRNA expression levels of key genes in the hematopoietic cell lineage, including (Cd38, Cd33, Il7r, Il2ra, Cd19), following hypoxanthine treatment, compared to control groups. The expression levels were normalized to GAPDH and analyzed across multiple time points. **(G-M)** Relative mRNA expression levels of genes involved in the MAPK signaling pathway, such as (Il1b, Dusp1, Map3k8, Fas, Hspa1a, Hspa1b, Tnf), after hypoxanthine treatment. Gene expression changes were assessed relative to the control group and normalized to GAPDH. Statistical significance was evaluated using one-way ANOVA followed by the Bonferroni post hoc test for multiple comparisons. Significance levels are indicated as follows: Data are presented as mean \pm SEM (**A-D**: $n = 6$; **E**: $n = 3$). Statistical significance was assessed using one-way ANOVA (Tukey's multiple comparisons test). * $P < 0.05$, ** $P < 0.01$, *** $P < 0.001$, **** $P < 0.0001$, and ns (not significant) $P \geq 0.05$

MAPK signal transduction by altering purine metabolism in the BM microenvironment, ultimately affecting hematopoietic fate.

Discussion

The immune suppression induced by microgravity poses significant challenges to long-duration space missions [27]. HSCs, as progenitor cells of the entire immune system, are essential for the continuous renewal and function of immune cells [28]. However, the effects of microgravity on HSCs functionality and their downstream differentiation into immune cells remain poorly understood. In this study, we utilized the HU model in mice to simulate the effects of microgravity on HSCs and immune cell composition [29]. Our findings reveal that microgravity induces a significant expansion of the HSCs population, particularly in LT-HSCs and ST-HSCs subtypes, while severely inhibiting the differentiation capacity of Hematopoietic stem and progenitor cells (HSPCs). This was accompanied by organ damage and disruptions

in peripheral blood cell composition in the mice, suggesting that microgravity impairs normal hematopoietic function. Furthermore, transcriptomic analysis of HSCs and metabolomic sequencing of the BM microenvironment identified 1631 DEGs and 58 DAMs, which were primarily enriched in the hematopoietic cell lineage and MAPK signaling pathways. Notably, alterations in the expression of key enzymes in the purine metabolism pathway, such as Entpd1, Entpd3, Nt5e, and Xdh, may be associated with the blockade of HSCs differentiation and immune dysfunction. Further molecular docking analyses and experimental validation confirmed that changes in the purine metabolism pathway within the BM microenvironment, particularly hypoxanthine, exhibit strong interactions with molecules involved in the MAPK signaling pathway and the hematopoietic cell lineage. These findings provide novel insights into how microgravity influences HSCs fate and gene expression, highlighting the role of metabolic alterations in the BM

microenvironment in regulating key signaling pathways that control hematopoietic fate.

In recent years, the effects of microgravity on the immune system have garnered widespread attention. NASA's twin study demonstrated that prolonged spaceflight may impact the health and function of HSCs and immune cells [30]. A recent study also revealed, through transcriptomic analysis of astronauts' blood samples, that there is an adaptive response in immune cell activity during long-term missions compared to pre-flight and post-flight conditions [31]. A longitudinal study by Pham et al. evaluated the health of HSCs and immune cells before and after space missions, finding that microgravity had a significant effect on immune cell health, with CD34⁺ cells showing marked adaptive changes during microgravity exposure [32]. These studies highlight the critical role of microgravity in modulating HSCs and immune cell function, providing valuable insights into the underlying cellular and molecular mechanisms.

Changes observed in peripheral blood often reflect deeper physiological and molecular processes occurring in hematopoietic tissues under spaceflight conditions. During the Spacelab 3 (SL-3) mission, a life sciences module carrying both young and mature rats was utilized to study the effects of spaceflight and microgravity on the hematological system. Hematological analysis revealed significant increases in HCT, RBC, and HGB in flight rats compared to ground-based controls. Furthermore, flight rats exhibited mild neutrophilia, lymphopenia, and a significant reduction in CFU-E counts in the bone marrow. These findings suggest that microgravity interferes with hematopoietic regulation in the bone marrow, leading to notable changes in blood parameters [33]. Our study further confirmed that HU, a well-established microgravity simulation model, induces significant increases in RBC and HGB in peripheral blood, alongside marked changes in HSCs within the BM. Cao et al. reported that after 28 days of HU treatment, the numbers of LT-HSCs, ST-HSCs, and MPPs significantly increased, while erythroid progenitor frequencies declined [34]. Similarly, our results demonstrated that HU treatment led to an increase in the proportions of LSK, LT-HSCs, and ST-HSCs, while MPP proportions decreased, indicating that HU activates HSCs and accelerates the differentiation of MPPs downstream. These findings highlight the impact of microgravity on HSCs activation and differentiation processes, ultimately affecting hematopoiesis.

Additionally, microgravity significantly suppresses the proliferation and differentiation of hematopoietic progenitor cells. Davis et al. cultured CD34⁺ BM progenitor cells with hematopoietic stromal support cells under microgravity/spaceflight and normal gravity conditions. After 11–13 days, total cell counts under microgravity conditions were reduced by 57–84% compared to

normal gravity. Microgravity significantly decreased the proportions of myeloid and erythroid progenitors, with erythroid progenitors showing the most pronounced suppression [35]. These observations are consistent with our findings in HU-treated mice, where the proportion of hematopoietic progenitor cells and the number of CFUs were significantly reduced.

The work of Vacek et al. further supports these findings, demonstrating that spaceflight reduces CFUs numbers in the BM, spleen, and liver of rats, irrespective of sex. Importantly, they found that the reduction in CFUs content in the BM of adult rats was not due to redistribution of these cells to the spleen or liver but rather the direct effects of microgravity. Following 14 days of spaceflight, CFU-GM and BFU-E in the BM were reduced by approximately 3–6 times and 1.5–2.5 times, respectively, compared to ground controls [36]. These results underscore the high sensitivity of BM CFUs to spaceflight conditions. Hodgson et al. proposed that the reduction in CFU-s numbers may result from their differentiation into more “mature” cellular forms. However, during spaceflight, this differentiation process appears insufficiently compensated by the recruitment of younger, more potent stem cells from the progenitor compartment. This suggests that microgravity not only directly disrupts HSCs proliferation and differentiation but may also impair the maturation process, leading to long-term suppression of hematopoietic function [37]. In summary, spaceflight and microgravity profoundly alter the proliferation and differentiation patterns of hematopoietic tissues, particularly impacting myeloid and erythroid progenitors.

This study reveals the profound impact of metabolic alterations within the BM microenvironment on the fate of HSCs. The immunometabolic landscape of the BM is closely intertwined with the health of HSCs [38], and metabolic imbalances can impair the differentiation potential of HSCs, leading to dysfunctions in the hematopoietic system [39]. Research by Salama et al. demonstrated that metabolic disruptions in the BM microenvironment directly affect HSCs function, particularly through regulatory factors involved in metabolic pathways. For instance, mutations in isocitrate dehydrogenase altered the polarization and functionality of BM macrophages, which in turn affected HSCs differentiation [40]. This study further supports the critical role of BM metabolism in regulating HSCs fate, especially under extreme conditions such as microgravity.

This study is the first to reveal that microgravity alters purine metabolism in the BM microenvironment, with hypoxanthine playing a critical role in microgravity-induced immunosuppression. Previous research has indicated that purine metabolism plays a pivotal role in HSCs fate decisions [41]. Ratajczak et al. proposed that metabolites in the BM microenvironment, such as

hypoxanthine and other purine metabolites, are essential not only for providing energy to HSCs but also for regulating their self-renewal and differentiation through signaling mechanisms [42]. It has been demonstrated that purine metabolism affects not only the differentiation of healthy HSCs but also the progression of pathological hematopoietic disorders [43]. Furthermore, Shi et al. highlighted the importance of purine metabolism in the maintenance of leukemia stem cells, where inhibiting this metabolic pathway promotes normal hematopoietic cell differentiation while reducing cancer cell proliferation [44]. In studies on HSCs aging, modulating uridine levels in purine metabolism has been shown to upregulate the FoxO signaling pathway, enhancing HSCs self-renewal and mitigating inflammation in aged HSCs [45].

This study identified a strong association between purine metabolism, hematopoietic cell lineage differentiation, and the MAPK signaling pathway, further validating the potential role of hypoxanthine in regulating HSCs differentiation via these pathways. Previous research has demonstrated that hypoxanthine is closely linked to the MAPK signaling pathway and plays a key role in regulating cell fate by influencing proliferation and differentiation [46]. Chen et al. reported that the MAPK signaling pathway is intricately connected to purine metabolism and serves as a critical step in regulating cellular proliferation and differentiation. In leukemia studies, inhibiting purine metabolism was shown to promote cell differentiation and reduce cancer cell proliferation [47], further supporting the relationship between hypoxanthine and the MAPK pathway. Both the hematopoietic cell lineage and MAPK signaling pathways are crucial in determining hematopoietic fate [48]. Studies by Koka and Ramdass demonstrated that the MAPK signaling pathway directly influences HSCs fate by regulating CD34⁺ cell differentiation. When MAPK signaling is suppressed, the cells' differentiation capacity significantly declines, leading to hematopoietic dysfunction [49]. These findings align with the results of the present study, confirming the essential role of the MAPK pathway in hematopoietic regulation. Li's research on the differentiation of induced pluripotent stem cells (iPSCs) into hematopoietic cells found that disruption of the MAPK pathway inhibited hematopoietic function derived from iPSCs, further corroborating the pathway's regulatory role in hematopoietic differentiation [50]. While these studies have uncovered the regulatory effects of the MAPK pathway in hematopoiesis [51], future research should further investigate the interactions between the MAPK and hematopoietic cell lineage pathways under various stress conditions, such as microgravity, and their long-term impact on HSCs fate.

The HU model is widely utilized to investigate the effects of microgravity on biological systems. In this study, the HU model successfully simulated

microgravity-induced impacts on HSCs, uncovering the molecular mechanisms by which microgravity inhibits HSCs differentiation. However, the HU model does not fully replicate the complexity of the space environment. Critical factors experienced by astronauts, such as space radiation and psychological stress, may also significantly influence HSCs behavior. For instance, Chang et al. demonstrated that space radiation can profoundly alter hematopoietic cell function through the generation of reactive oxygen species (ROS) [52]. Similarly, psychological stress may disrupt bone marrow microenvironment stability via neuroendocrine pathways [53]. Additionally, complementary models, such as in vitro cell-based systems and rotary wall vessel (RWV) bioreactors for simulating microgravity, can provide a broader perspective on the factors influencing HSC function [54]. Future research should integrate these complementary models to offer a more comprehensive understanding of the multifaceted influences on HSCs under spaceflight conditions. Furthermore, validating these findings in actual spaceflight environments will enhance the translational relevance and applicability of this study's results to real-world space missions.

The regulation of purine metabolism has been demonstrated to have therapeutic potential in various physiological and pathological contexts. For instance, studies have shown that modulating the activity of key enzymes in purine metabolism, such as Xdh or Nt5e, can significantly enhance hematopoietic function [55]. Additionally, pharmacological strategies targeting hypoxanthine levels, including the use of known hypoxanthine scavengers or inhibitors of its metabolic pathways, have emerged as promising therapeutic approaches [56]. Zeng, et al. [57] highlighted that the MAPK signaling pathway plays a pivotal role as a regulatory node for hypoxanthine-mediated cell fate decisions. This suggests that combined modulation of the MAPK pathway and purine metabolism may offer synergistic therapeutic benefits. Future research should focus on exploring the therapeutic potential of this metabolic-signaling pathway interaction and developing interventions targeting hypoxanthine or purine metabolism to mitigate microgravity-induced immunosuppression and hematopoietic dysfunction.

Conclusion

This study systematically revealed, for the first time, the profound impact of microgravity on HSCs function and immune homeostasis, highlighting the critical role of purine metabolism in this process. By integrating transcriptomic and metabolomic analyses, the research offers new directions for investigating the effects of microgravity on the immune system. These findings not only enhance our understanding of the mechanisms underlying microgravity-induced immunosuppression but also

provide a theoretical foundation for maintaining immune function during future space exploration missions.

Abbreviations

ANOVA	Analysis of variance
BP	Biological processes
BM	Bone marrow
BMC	Bone mineral content
BFU-E	Burst-forming unit-erythroid
CC	Cellular component
CFU-GEMM	CFU granulocyte-erythrocyte-macrophage-megakaryocyte
CFU-GM	CFU granulocyte-macrophage
CFU	Colony-forming unit
CLPs	Common lymphoid progenitors
CMPs	Common myeloid progenitors
CON	Control group
DAMs	Differentially accumulated metabolites
DEGs	Differentially expressed genes
EMH	Extramedullary hematopoiesis
FDR	False discovery rates
GMPs	Ganulocyte-macrophage progenitors
GO	Gene ontology
GSEA	Gene set enrichment analysis
HSPCs	Hematopoietic stem and progenitor cells
HSCs	Hematopoietic stem cells
H&E	Hematoxylin and eosin
HGB	Hemoglobin
HU	Hindlimb unloading
KEGG	Kyoto Encyclopedia of Genes and Genomes
LSK	Lin ⁻ Sca-1 ⁺ c-kit ⁺
LT-HSCs	Long-term HSCs
LYM	Lymphocyte
LC-MS	liquid chromatograph mass spectrometer
MEPs	Megakaryocyte-erythroid progenitors
MF	Molecular functions
MPPs	Multipotent progenitors
NES	Normalized enrichment scores
OPLS-DA	Orthogonal partial least squares discriminant analysis
PBS	Phosphate-buffered saline
PLT	Platelet
iPSCs	Pluripotent stem cells
PCA	Principal component analysis
RBC	Red blood cell
RP	Red pulp
RNA-Seq	RNA sequencing
ROS	Reactive oxygen species
RWV	Rotary wall vessel
ST-HSCs	Short-term HSCs
SEM	Standard error of the mean
TIC	Total ion chromatograms
UPLC	Ultra-performance liquid chromatography
WBC	White blood cell
WP	White pulp
Xdh	Xanthine dehydrogenase

Supplementary Information

The online version contains supplementary material available at <https://doi.org/10.1186/s13287-025-04213-9>.

Supplementary Material 1

Acknowledgements

The authors acknowledge the all members of the Research Center of Special Environmental Biomechanics and Medical Engineering at Northwestern Poly technical University. The authors express our gratitude to all the projects that have offered their support to facilitate this study. Furthermore, the authors declare that we have not use AI-generated work in this manuscript.

Author contributions

Xiru Liu: Data curation, Writing– original draft. Hao Zhang: Formal analysis. Jinxiao Yan and Penghui Ye: Methodology. Yanran Wang: Resources. Nu Zhang and Zhenhao Tian: Supervision. Bin Liu: Software. Hui Yang: Funding acquisition, Investigation, Writing– review & editing.

Funding

This work was supported by grants from the National Natural Science Foundation of China (12002285), the Natural Science Foundation of Shaanxi (2020JZ-11, 2022JQ-059), the National Natural Science Foundation of China (32101202), the Fundamental Research Funds for the Central Universities (G2024KY05106) and the Innovation Foundation for Doctor Dissertation of Northwestern Polytechnical University (CX2023077).

Data availability

All data relevant to the study are included in the article or uploaded as online supplemental information.

Declarations

Institutional review board statement

The ethics approval for the research project titled “Effect of microgravity environment on proliferation and differentiation of hematopoietic stem cells in mice” was granted by the Medical and Laboratory Animal Ethics Committee of Northwestern Polytechnical University. The approval number for this project is 202401196, and the date of approval is September 20, 2024. All animals involved in the study were handled in accordance with ethical guidelines, and their care and use were approved by the Medical and Laboratory Animal Ethics Committee of Northwestern Polytechnical University.

Competing interest

The authors report no conflicts of interest. The authors alone are responsible for the content and writing of the paper.

Author details

¹School of Life Sciences, Northwestern Polytechnical University, Xi’an, China

²Engineering Research Center of Chinese Ministry of Education for Biological Diagnosis, Treatment and Protection Technology and Equipment, Xi’an, China

³Research Center of Special Environmental Biomechanics and Medical Engineering, Northwestern Polytechnical University, Xi’an, China

⁴Department of Infectious Diseases, Characteristic Medical Center of Chinese People’s Armed Police Forces, Tianjin, China

Received: 18 December 2024 / Accepted: 30 January 2025

Published online: 05 March 2025

References

- Jillings S, et al. Macro- and microstructural changes in cosmonauts’ brains after long-duration spaceflight. *Sci Adv*. 2020;6. <https://doi.org/10.1126/sciadv.aaz9488>.
- Saleem I, et al. Adhesion of gram-negative rod-shaped bacteria on 1D nano-ripple glass pattern in weak magnetic fields. *Microbiologyopen*. 2019;8:e00640. <https://doi.org/10.1002/mbo3.640>.
- Zeng LL, et al. Default network connectivity decodes brain states with simulated microgravity. *Cogn Neurodyn*. 2016;10:113–20. <https://doi.org/10.1007/s11571-015-9359-8>.
- Shi L, et al. Spaceflight and simulated microgravity suppresses macrophage development via altered RAS/ERK/NFkappaB and metabolic pathways. *Cell Mol Immunol*. 2021;18:1489–502. <https://doi.org/10.1038/s41423-019-0346-6>.
- Acharya A, et al. Modulation of differentiation processes in murine embryonic stem cells exposed to Parabolic Flight-Induced Acute Hypergravity and Microgravity. *Stem Cells Dev*. 2018;27:838–47. <https://doi.org/10.1089/scd.2017.0294>.
- Morabito C, et al. Antioxidant strategy to prevent simulated Microgravity-Induced effects on bone osteoblasts. *Int J Mol Sci*. 2020;21. <https://doi.org/10.3390/ijms21103638>.

7. Chang TT, et al. The Rel/NF-kappaB pathway and transcription of immediate early genes in T cell activation are inhibited by microgravity. *J Leukoc Biol*. 2012;92:1133–45. <https://doi.org/10.1189/jlb.0312157>.
8. Yamashita M, Passegue E. 2019. TNF-alpha coordinates hematopoietic stem cell survival and myeloid regeneration. *Cell Stem Cell*. 25: 357–372.e7. <https://doi.org/10.1016/j.stem.2019.05.019>
9. Wang P, et al. Spaceflight/microgravity inhibits the proliferation of hematopoietic stem cells by decreasing Kit-Ras/cAMP-CREB pathway networks as evidenced by RNA-Seq assays. *FASEB J*. 2019;33:5903–13. <https://doi.org/10.1096/fj.201802413R>.
10. Li L, et al. Effects of simulated microgravity on the expression profiles of RNA during osteogenic differentiation of human bone marrow mesenchymal stem cells. *Cell Prolif*. 2019;52:e12539. <https://doi.org/10.1111/cpr.12539>.
11. Wang L, et al. Mechanical sensing protein PIEZO1 regulates bone homeostasis via osteoblast-osteoclast crosstalk. *Nat Commun*. 2020;11:282. <https://doi.org/10.1038/s41467-019-14146-6>.
12. Mattiucci D, et al. Bone marrow adipocytes support hematopoietic stem cell survival. *J Cell Physiol*. 2018;233:1500–11. <https://doi.org/10.1002/jcp.26037>.
13. Cuminetti V, Arranz L. Bone marrow adipocytes: the Enigmatic Components of the hematopoietic stem cell niche. *J Clin Med*. 2019;8. <https://doi.org/10.3390/jcm8050707>.
14. Maynard RS, et al. Acute myeloid leukaemia drives metabolic changes in the bone marrow niche. *Front Oncol*. 2022;12:924567. <https://doi.org/10.3389/fonc.2022.924567>.
15. Bennett BT et al. The Effects of Calcium-beta-Hydroxy-beta-Methylbutyrate on Aging-Associated Apoptotic Signaling and Muscle Mass and Function in Unloaded but Nonatrophied Extensor Digitorum Longus Muscles of Aged Rats. *Oxid Med Cell Longev*. 2020: 3938672. <https://doi.org/10.1155/2020/3938672>
16. Morey-Holton ER et al. Hindlimb unloading of growing rats: a model for predicting skeletal changes during space flight. *Bone*. 1998;22:835–885. [https://doi.org/10.1016/s8756-3282\(98\)00019-2](https://doi.org/10.1016/s8756-3282(98)00019-2). S-885.
17. Sakr HF, et al. Resveratrol modulates bone Mineral Density and Bone Mineral content in a rat model of male hypogonadism. *Chin J Integr Med*. 2023;29:146–54. <https://doi.org/10.1007/s11655-022-2895-2>.
18. Ge Y, et al. Discovery of Salidroside as a Novel non-coding RNA modulator to Delay Cellular Senescence and promote BK-Dependent apoptosis in cerebrovascular smooth muscle cells of simulated microgravity rats. *Int J Mol Sci*. 2023;24. <https://doi.org/10.3390/ijms241914531>.
19. Guo H, et al. Multi-omics analyses of radiation survivors identify radioprotective microbes and metabolites. *Science*. 2020;370. <https://doi.org/10.1126/science.aay9097>.
20. Farahzadi R, et al. Granulocyte differentiation of rat bone marrow resident C-kit(+) hematopoietic stem cells induced by mesenchymal stem cells could be considered as new option in cell-based therapy. *Regen Ther*. 2023;23:94–101. <https://doi.org/10.1016/j.reth.2023.04.004>.
21. Maadi H, et al. Analysis of cell cycle by Flow Cytometry. *Methods Mol Biol*. 2022;2579:183–95. https://doi.org/10.1007/978-1-0716-2736-5_14.
22. Yang W, et al. PRAS40 alleviates neurotoxic prion peptide-induced apoptosis via mTOR-AKT signaling. *CNS Neurosci Ther*. 2017;23:416–27. <https://doi.org/10.1111/cns.12685>.
23. Managlia E, et al. Blocking NF-kappaB activation in Ly6c(+) monocytes attenuates necrotizing enterocolitis. *Am J Pathol*. 2019;189:604–18. <https://doi.org/10.1016/j.ajpath.2018.11.015>.
24. Zhang Z, et al. Bone marrow adipose tissue-derived stem cell factor mediates metabolic regulation of hematopoiesis. *Haematologica*. 2019;104:1731–43. <https://doi.org/10.3324/haematol.2018.205856>.
25. Fathi E, et al. Mesenchymal stem cells as a cell-based therapeutic strategy targeting the telomerase activity of KG1 acute myeloid leukemia cells. *Acta Medica Iranica*. 2022;60:2. <https://doi.org/10.18502/acta.v60i2.8817>
26. Kunz H, et al. Alterations in hematologic indices during long-duration spaceflight. *BMC Hematol*. 2017;17:12. <https://doi.org/10.1186/s12878-017-0083-y>.
27. Singh NK, et al. Succession and persistence of microbial communities and antimicrobial resistance genes associated with International Space Station environmental surfaces. *Microbiome*. 2018;6:204. <https://doi.org/10.1186/s40168-018-0585-2>.
28. Leins H, et al. Aged murine hematopoietic stem cells drive aging-associated immune remodeling. *Blood*. 2018;132:565–76. <https://doi.org/10.1182/blood-2018-02-831065>.
29. Tyganov SA, et al. Effects of Plantar Mechanical Stimulation on Anabolic and Catabolic Signaling in Rat Postural muscle under short-term simulated gravitational unloading. *Front Physiol*. 2019;10:1252. <https://doi.org/10.3389/fphys.2019.01252>.
30. Garrett-Bakelman FE, et al. The NASA Twins Study: a multidimensional analysis of a year-long human spaceflight. *Science*. 2019;364. <https://doi.org/10.1126/science.aau8650>.
31. Stratis D, et al. The transcriptome response of astronaut leukocytes to long missions aboard the International Space Station reveals immune modulation. *Front Immunol*. 2023;14:1171103. <https://doi.org/10.3389/fimmu.2023.1171103>.
32. Pham J, et al. A longitudinal study to assess hematopoietic stem cell and Immune Cell Health in astronauts Pre-, during, and Post-mission. *Blood*. 2023;142:4056. <https://doi.org/10.1182/blood-2023-187749>.
33. Lange RD, et al. Hematological measurements in rats flown on Spacelab shuttle, SL-3. *Am J Physiol*. 1987;252:R216–21. <https://doi.org/10.1152/ajpregu.1987.252.2.R216>
34. Cao D et al. Hematopoietic stem cells and lineage cells undergo dynamic alterations under microgravity and recovery conditions. *The FASEB Journal*. 2019;33:6904–18. <https://doi.org/10.1096/fj.201802421RR>
35. Davis TA, et al. Effect of spaceflight on human stem cell hematopoiesis: suppression of erythropoiesis and myelopoiesis. *J Leukoc Biol*. 1996;60:69–76. <https://doi.org/10.1002/jlb.60.1.69>.
36. Vacek A, et al. Changes in the number of haemopoietic stem cells (CFUs) in bone marrow and spleens of pregnant rats after a short space flight onboard the Cosmos-1514 biosatellite. *Folia Biol (Praha)*. 1985;31:361–5.
37. Hodgson GS, Bradley TR. Properties of haematopoietic stem cells surviving 5-fluorouracil treatment: evidence for a pre-CFU-S cell? *Nature*. 1979;281:381–2. <https://doi.org/10.1038/281381a0>.
38. Sago CD, et al. Nanoparticles that deliver RNA to bone marrow identified by in vivo Directed Evolution. *J Am Chem Soc*. 2018;140:17095–105. <https://doi.org/10.1021/jacs.8b08976>.
39. Salama NA, et al. Isocitrate dehydrogenase 2 mutation allows myeloid differentiation but impairs bone marrow macrophage polarization and function Via Metabolic Dysregulation. *Blood*. 2023;142:314. <https://doi.org/10.1182/blood-2023-190617>.
40. Xu RJC, Discovery T. Impacts of immune microenvironment on musculoskeletal health. *Clin Translational Discovery*. 2024;4:e290. <https://doi.org/10.1002/ctd2.290>.
41. Karigane D, et al. p38α activates purine metabolism to initiate hematopoietic stem/progenitor cell cycling in response to stress. *Cell Stem Cell*. 2016;19:192–204. <https://doi.org/10.1016/j.stem.2016.05.013>.
42. Ratajczak MZ, et al. Hematopoiesis revolves around the primordial evolutionary rhythm of purinergic signaling and innate immunity—a journey to the developmental roots. *Stem Cell Reviews Rep*. 2024;20:827–38. <https://doi.org/10.1007/s12015-024-10692-9>.
43. Suda TJB. Purine metabolism and hematopoietic stem and progenitor stem cells under stress. *Blood*. 2018;132:SCI–19. <https://doi.org/10.1182/blood-2018-99-109515>
44. Shi X, et al. Purine metabolism modulates leukemia stem cell maintenance in MLL-rearranged acute leukemia. *Blood*. 2023;142:582. <https://doi.org/10.1182/blood-2023-190833>.
45. Zeng X, et al. A metabolic atlas of blood cells in young and aged mice identifies uridine as a metabolite to rejuvenate aged hematopoietic stem cells. *Nat Aging*. 2024;1–16. <https://doi.org/10.1038/s43587-024-00669-1v>.
46. Aboali M, et al. Crucial involvement of xanthine oxidase in the intracellular signalling networks associated with human myeloid cell function. *Sci Rep*. 2014;4:6307. <https://doi.org/10.1038/srep06307>.
47. Chen H, et al. Kdm6a modulates hematopoiesis and Leukemogenesis Via demethylase-dependent epigenetic programming. *Blood*. 2023;142:1372. <https://doi.org/10.1182/blood-2023-188635>.
48. Hurwitz SN, et al. Hematopoietic stem and progenitor cell signaling in the niche. *Leukemia*. 2020;34:3136–48. <https://doi.org/10.1038/s41375-020-01062-8>.
49. Koka PS, et al. MicroRNA target homeobox messenger RNA in HIV induced hematopoietic inhibition. *Front Cell Dev Biology*. 2024;12:1382789. <https://doi.org/10.3389/fcell.2024.1382789>.
50. Li Y, et al. Modulation of WNT, Activin/Nodal, and MAPK signaling pathways increases arterial hemogenic endothelium and hematopoietic Stem/Progenitor cell formation during human iPSC differentiation. *Stem Cells*. 2023;41:685–97. <https://doi.org/10.1093/stmcls/sxad040>.
51. Singh AK, et al. Signaling pathways regulating hematopoietic stem cell and progenitor aging. *Curr Stem Cell Rep*. 2018;4:166–81. <https://doi.org/10.1007/s40778-018-0128-6>.

52. Chang J, et al. Low doses of Oxygen Ion Irradiation cause Acute damage to hematopoietic cells in mice. *PLoS ONE*. 2016;11:e0158097. <https://doi.org/10.1371/journal.pone.0158097>.
53. Kollet O, et al. Physiologic corticosterone oscillations regulate murine hematopoietic stem/progenitor cell proliferation and CXCL12 expression by bone marrow stromal progenitors. *Leukemia*. 2013;27:2006–15. <https://doi.org/10.1038/leu.2013.154>.
54. Anil-Inevi M, et al. Stem cell culture under simulated microgravity. *Adv Exp Med Biol*. 2020;1298:105–32. https://doi.org/10.1007/5584_2020_539.
55. Schultz IC, et al. Purinergic signaling elements are correlated with coagulation players in peripheral blood and leukocyte samples from COVID-19 patients. *J Mol Med (Berl)*. 2022;100:569–84. <https://doi.org/10.1007/s00109-021-02175-y>.
56. Chaves NA, et al. Impaired antioxidant capacity causes a disruption of metabolic homeostasis in sickle erythrocytes. *Free Radic Biol Med*. 2019;141:34–46. <https://doi.org/10.1016/j.freeradbiomed.2019.05.034>.
57. Zeng X, et al. Metabolism in Hematopoiesis and its malignancy. *Adv Exp Med Biol*. 2023;1442:45–64. https://doi.org/10.1007/978-981-99-7471-9_4.

Publisher's note

Springer Nature remains neutral with regard to jurisdictional claims in published maps and institutional affiliations.